

Regional aerosol properties: Comparisons of boundary layer measurements from ACE 1, ACE 2, Aerosols99, INDOEX, ACE Asia, TARFOX, and NEAQS

Patricia K. Quinn and Timothy S. Bates

Pacific Marine Environmental Laboratory, NOAA, Seattle, Washington, USA

Received 10 March 2004; revised 17 September 2004; accepted 25 January 2005; published 23 July 2005.

[1] Means and variability of aerosol chemical composition and optical properties are compared for the first and second Aerosol Characterization Experiments (ACE 1 and ACE 2), a cruise across the Atlantic (Aerosols99), the Indian Ocean Experiment (INDOEX), the Asian Aerosol Characterization Experiment (ACE Asia), the Tropospheric Aerosol Radiative Forcing Observational Experiment (TARFOX), and the New England Air Quality Study (NEAQS). These experiments were focused either on the remote marine atmosphere (ACE 1) or areas downwind of continental aerosol source regions including western Europe, North America, Africa, India, and Asia. Presented here are size-segregated concentrations of aerosol mass, sea salt, non-sea-salt (nss) SO_4^- , NH_4^+ , NO_3^- , dust, organic carbon (OC), elemental carbon (EC), and nss K^+ , as well as mass ratios that are commonly used to identify aerosol sources and to assess aerosol processing (Cl^- to Na^+ , OC to nss SO_4^- , EC to total carbon (TC), EC to nss SO_4^- , nss K^+ to EC, Fe to Al, and Si to Al). Optical properties that are compared include size-segregated scattering, backscattering, and absorption coefficients, and single-scattering albedo at 550 nm. Size-segregated mass scattering and mass absorption efficiencies for the total aerosol and mass extinction efficiencies for the dominant chemical components also are compared. In addition, we present the contribution to light extinction by the dominant chemical components for each region. All data are based on shipboard measurements performed at a relative humidity of $55 \pm 5\%$. Scattering coefficients and single-scattering albedos also are reported at ambient relative humidity (RH) using published values of $f(\text{RH})$. Finally, aerosol optical depths from each region are compared. Identical sampling protocols were used in all experiments in order to eliminate sampling biases and to make the data directly comparable. Major findings include (1) nss SO_4^- makes up only 16 to 46% of the submicron aerosol mass, which means there is a large and variable fraction of the aerosol that is not sulfate, (2) particulate organic matter (POM) makes up 1 to 51% of the submicron mass, with highest POM mass fractions observed downwind of the NE United States, (3) highest submicron mass fractions of EC and lowest single-scattering albedos were observed in biomass-burning plumes from Africa and downwind of the Indian subcontinent, (4) NO_3^- was found predominantly in the supermicron size range due to the interaction of gas phase oxidized nitrogen species with sea salt aerosol, and (5) mass extinction efficiencies for the individual chemical components were consistent between regions. All data presented are available as auxiliary material.

Citation: Quinn, P. K., and T. S. Bates (2005), Regional aerosol properties: Comparisons of boundary layer measurements from ACE 1, ACE 2, Aerosols99, INDOEX, ACE Asia, TARFOX, and NEAQS, *J. Geophys. Res.*, 110, D14202, doi:10.1029/2004JD004755.

1. Introduction

[2] Since 1995, there have been many field experiments focused on the characterization of tropospheric aerosol properties to improve estimates of aerosol direct radiative forcing of climate. Several of these experiments have been located in marine environments immediately downwind

of known continental aerosol source regions and have involved intensive field operations with measurements from ships, aircraft, and coastal land sites. Measurements over the ocean are prompted by satellite observations of backscattered radiation that reveal persistent seasonal aerosol plumes downwind of continents and the relative ease of accounting for the surface albedo over a uniform, dark ocean compared with inhomogeneous, bright land surfaces. In situ shipboard measurements have played an important role in these

This paper is not subject to U.S. copyright.
Published in 2005 by the American Geophysical Union.

experiments, as they provide information about aerosol chemical composition, size distributions, optical properties, and mass loadings in the boundary layer. This information is required to fully understand the impact of regional aerosol plumes on climate and air quality.

[3] This paper presents a comparison of the means and variability in regional aerosol chemical and optical properties based on shipboard measurements during the following experiments (Figure 1). The first Aerosol Characterization Experiment (ACE 1) took place in the Southern Ocean environment south of Australia and was designed to avoid continental plumes [Bates *et al.*, 1998a, 1998b]. The goal was to characterize the “background” aerosol upon which anthropogenic forcings could be imposed. The second Aerosol Characterization Experiment (ACE 2) took place in the subtropical northeast Atlantic Ocean and focused on the European plume [Raes *et al.*, 2000]. Aerosols99 was a transit cruise across the Atlantic from Norfolk, Virginia, USA to Cape Town, South Africa [Bates *et al.*, 2001]. Along the cruise track, aerosols from dust and biomass-burning source regions within Africa were encountered. The Indian Ocean Experiment (INDOEX) characterized the plumes emanating from the Indian subcontinent and nearby regions as they were transported out over the Indian Ocean [Ramanathan *et al.*, 2001]. The Asian Aerosol Characterization Experiment (ACE Asia) focused on the plume downwind of Asia [Huebert *et al.*, 2003]. The Tropospheric Aerosol Radiative Forcing Observational Experiment (TARFOX) [Russell *et al.*, 1999] and the New England Air Quality Study (NEAQS) focused on the eastern U.S. plume. Table 1 lists the details of these experiments.

[4] Results from these experiments have been reported or soon will be reported in a variety of peer-reviewed journals. Our goal is not to summarize already-reported results here. Instead, we capitalize on our unique perspective of having participated in all of these experiments (with the exception of TARFOX) and having used standardized sampling protocols throughout in order to minimize sampling biases. Hence data from the different regions are directly comparable. The comparisons shown here are valuable for several reasons. They indicate the aerosol optical and chemical properties that have the largest regional variability and therefore the largest potential impact on the accuracy of air quality forecast and climate models. They indicate the relative importance of the aerosol sources that impact specific regions, and they can aid in the design of regional experiments by pointing out measurement and knowledge gaps. In addition, the data that are presented can be used to validate chemical transport and radiative transfer models for specific locations and times. For this reason, we have made the data shown in the figures and tables in this article available in the form of an electronic supplement¹. Complete data sets for all times and parameters measured during each experiment are available at <http://saga.pmel.noaa.gov/data>.

[5] Aerosol chemical properties that are compared include mass fractions of the dominant chemical components, where mass fraction is defined as the mass concentration of the chemical component divided by the total aerosol mass. Mass fractions indicate the relative importance of aerosol

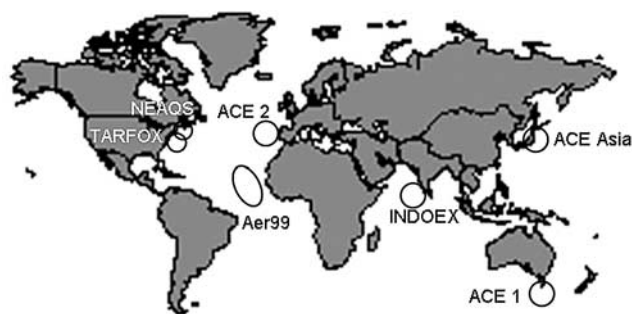


Figure 1. Regional map of experiments. Details of the experiments are given in Table 1.

sources within each region. The chemical components in this analysis include NH_4^+ , nss SO_4^- , NO_3^- , sea salt, particulate organic matter (POM), elemental carbon (EC), nss K^+ , dust, and H_2O . Mass fractions are presented for the submicron, supermicron, and sub- $10\ \mu\text{m}$ size ranges. Also presented are the means and variability of the mass concentrations of the dominant chemical components and mass ratios of select chemical species for each region. Mass ratios are useful in identifying regional aerosol sources and validating chemical transport models.

[6] The extensive aerosol optical properties that are compared include light scattering and absorption by sub- $10\ \mu\text{m}$ aerosol and aerosol optical depth (AOD). Intensive optical properties include the fraction of the sub- $10\ \mu\text{m}$ aerosol light scattering due to particles less than $1\ \mu\text{m}$ in diameter (termed here the fine fraction of scattering or FF_{scat}). This quantity is useful in identifying whether fine (roughly submicron) or coarse (roughly supermicron) particles are dominating light scattering for a particular region and meteorological situation. Additional intensive optical properties include the submicron and sub- $10\ \mu\text{m}$ backscattered fraction or the fraction of the scattered light that is redirected into the backward hemisphere of the particle. This quantity can be used to approximate the fraction of scattered sunlight that is scattered into the upward hemisphere away from the Earth. Submicron and sub- $10\ \mu\text{m}$ single-scattering albedo (SSA) at 55% relative humidity (RH) and ambient RH also are compared. Each of these optical properties is used directly or implicitly in calculating the direct radiative forcing by tropospheric aerosol. Hence the data presented here are useful for validating radiative transfer models and aerosol properties retrieved from satellite and surface-based remote-sensing observations.

[7] The final regional comparisons are of mass extinction efficiencies for the total aerosol and the dominant aerosol chemical components and the extinction fractions of the chemical components. Mass extinction efficiency is defined as the light extinction due to the total aerosol or an individual aerosol chemical component per unit mass. An extinction fraction is the ratio of the light extinction due to a chemical component divided by the total measured aerosol light extinction. Both mass extinction efficiencies and extinction fractions link aerosol sources to aerosol direct radiative effects.

[8] All data are reported at the measurement RH of $55 \pm 5\%$. Scattering coefficients and single-scattering albedo also are reported at ambient RH.

¹Auxiliary material is available at <ftp://ftp.agu.org/apend/jd/2004JD004755>.

Table 1. Field Experiments Focused on Determining the Impact of Aerosol Plumes on Regional Atmospheric Chemistry and Climate

Experiment	Identifier	Region of Measurements Reported Here	Distance from Upwind Shore, km	Dates	References
ACE 1	ACE 1	Southern Ocean south of Australia		Nov–Dec 1995	<i>Bates et al.</i> [1998a, 1998b], <i>Quinn et al.</i> [1998]
ACE 2	ACE 2 Cont ^a	Sub-tropical NE Atlantic	2 to 900	Jun–Jul 1997	<i>Raes et al.</i> [2000], <i>Quinn et al.</i> [2000]
Aerosols99	AER99 Dust ^b AER99 BB ^c	Tropical Atlantic	1200 to 1400 160 to 960	Jan–Feb 1999	<i>Bates et al.</i> [2001], <i>Quinn et al.</i> [2001]
INDOEX	IND Arabia ^d IND India ^e	Northern Indian Ocean	900 to 1400	Jan–Mar 1999	<i>Ramanathan et al.</i> [2001], <i>Quinn et al.</i> [2002]
ACE Asia	AA Poll ^f AA Poll + Dust ^g	E. Coast of Japan, Sea of Japan, E. China Sea	100 to 400	Mar–Apr 2001	<i>Huebert et al.</i> [2003], <i>Quinn et al.</i> [2004]
TARFOX	TAR Cont ^{a,h}	U.S. Eastern Seaboard (37° to 39°N)	≤150	July 1996	<i>Russell et al.</i> [1999]
NEAQS	NEAQS Cont ^a	U.S. Eastern Seaboard (33° to 45°N)	20 to 100	Jul–Aug 2002	<i>Quinn and Bates</i> [2003]

^aCont = Trajectories indicate the sampled air masses had recent (<2 days) contact with continental regions with known sources of pollution and/or dust regions.

^bSamples were collected between 15.5° and 8°N. Trajectories indicate the sampled air masses had recent (<2 days) contact with African dust source regions.

^cSamples were collected between 3°N and 5°S. BB = biomass burning.

^dTrajectories indicate the sampled air masses had recent (<2 days) contact with Arabia.

^eTrajectories indicate the sampled air masses had recent (<2 days) contact with the Indian subcontinent.

^fPoll = Trajectories indicate the sampled air masses had recent (<2 days) contact with Asian continental regions with known sources of pollution.

^gPoll + Dust = Trajectories indicate the sample air masses had recent (<2 days) contact Asian continental regions with known sources of pollution and dust.

^hTARFOX was an aircraft-based experiment. Only samples collected at altitudes <300 m were included in this analysis.

[9] With the exception of Aerosols99, the experiments included in this analysis were conducted during the time of year when the targeted aerosol plume was expected to be most pronounced. As a result, the range of reported values most likely is skewed toward the higher values typical of these seasonally maximum plumes. In addition, the reported variability reflects only that which was measured during these short-lived campaigns. There is evidence for some of these experiments that the data are representative of other years. Results from the 1999 INDOEX field campaign are expected to be representative of other years based on satellite data for 1996 to 2000 [*Ramanathan et al.*, 2001]. Seasonally (January to March) and spatially (0° to 30°N) averaged AOD for these 5 years varied by less than 10% of the 1999 values. Similarly, the summer mean values of AOD measured at Greenbelt, Maryland, a site in the mid-Atlantic region of the U.S., varied by less than 15% between 1993 and 1996, indicating that the 1996 TARFOX values were representative of other years [*Remer et al.*, 1999]. In addition, the mean regional AOD measured during NEAQS was within 18% of regional mean summer values derived from five Aeronet sites along the mid-Atlantic coast in 1993 and 1996 [*Remer et al.*, 1999]. The dust storms sampled during ACE Asia were part of a major event that extended across the Pacific, North America, and the Atlantic [*Huebert et al.*, 2003]. Hence the ACE Asia time period may represent an upper bound of dust impacts on aerosol chemical composition and optical properties.

[10] The distance of the measurements from the upwind continental haze source must also be considered when comparing the regional aerosol properties. Over all experiments, this distance ranged from 2 to 1400 km (Table 1). For all experiments except ACE 1, back trajectories indicated that the travel time from the upwind shore to the measurement platform was ≤3 days. The global estimate of the average lifetime of sulfate aerosol is about 5 days [*Langner and Rodhe*, 1991]. During INDOEX, the aerosol

lifetime was estimated to be 7 to 8 days due to a lack of wet deposition [*Rasch et al.*, 2001]. Similarly dry conditions during NEAQS and ACE Asia are expected to have led to equivalent lifetimes. For conditions of little or no dilution of air from mixing across the marine boundary layer inversion, the short transport times relative to the aerosol lifetime should yield a fairly constant concentration of particulates in the plume 100 to 1400 km from shore. The uniformity of the aerosol concentration downwind of India is confirmed by satellite-derived average AOD for a 2 week period during INDOEX [*Collins et al.*, 2001]. Values range from 0.35 to 0.4 for the region extending westward from the coast of India to 68°E longitude. This region encompassed the ship cruise track.

[11] As stated above, the same sampling protocol was used for ACE 1, ACE 2, Aerosols99, INDOEX, ACE Asia, and NEAQS to eliminate biases in the data due to sampling and analysis methods. The sampling protocol involved using the same aerosol inlet for all cruises and measuring all aerosol properties from this common inlet. In addition, the sample air was maintained at a constant reference RH of 55 ± 5%. A stable reference RH allows for constant instrumental size segregation in spite of variations in ambient RH and results in chemical and optical measurements which are directly comparable. In addition, measurement at a constant reference RH makes it possible, with the knowledge of appropriate growth factors, for end users of the data set (process, chemical transport, and radiative transfer models) to adjust the measured parameters to a desired RH. An RH of 55% was chosen because it is above the crystallization humidity of most aerosol component and component mixtures [*Carrico et al.*, 2003; *Shaw and Rood*, 1990]. Identical submicron or sub-10 μm impactors upstream of all instruments further ensured that all instruments sampled the same particle size range. Although different sampling protocols were used during TARFOX, we include it in this analysis since it took place in the vicinity of

NEAQS and contributes to the eastern U.S. plume data set. Since TARFOX was an aircraft study, we include only data collected at altitudes less than or equal to 300 m.

2. Methods

2.1. Aerosol Inlet

[12] Sample air for all measurements was drawn through a 6-m mast. The entrance to the mast was 10 to 18 m above sea level and forward of the ship's stack. The transmission efficiency of the inlet for particles with aerodynamic diameters less than 6.5 μm (the largest size tested) is greater than 95% [Bates *et al.*, 2002]. Air was sampled only when the particle number concentration, the relative wind speed, and the relative wind direction all indicated that there was no possibility of contamination from the ship's stack. All measurements were made at $55 \pm 5\%$ RH.

2.2. Aerosol Chemical Composition: Inorganic Ions

[13] Two-stage multijet cascade impactors [Bernier *et al.*, 1979] were used to determine submicron and supermicron concentrations of aerosol mass, inorganic ions, OC and EC, and inorganic oxidized material (IOM). The 50% aerodynamic cutoff diameters of the impactors, $D_{50,\text{aero}}$, were 1.1 and 10 μm . The RH of the sampled air stream was measured a few centimeters upstream from the impactors. Throughout the paper, submicron refers to particles with $D_{\text{aero}} < 1.1 \mu\text{m}$ at 55% RH and supermicron refers to particles with $1.1 \mu\text{m} < D_{\text{aero}} < 10 \mu\text{m}$ at 55% RH. Sub-10 μm refers to particles with $D_{\text{aero}} < 10 \mu\text{m}$ at 55% RH. Details of sample handling and blank determination can be found in the work of Quinn *et al.* [2002].

[14] Concentrations of Cl^- , NO_3^- , SO_4^{2-} , Na^+ , NH_4^+ , K^+ , Mg^{+2} , and Ca^{+2} were determined by ion chromatography (IC) [Quinn *et al.*, 1998]. Non-sea-salt sulfate concentrations were calculated from Na^+ concentrations and the ratio of sulfate to sodium in seawater. Sea salt aerosol concentrations were calculated as

$$\text{Sea salt}(\mu\text{g m}^{-3}) = \text{Cl}^-(\mu\text{g m}^{-3}) + \text{Na}^+(\mu\text{g m}^{-3}) \times 1.47 \quad (1)$$

where 1.47 is the seawater ratio of $(\text{Na}^+ + \text{K}^+ + \text{Mg}^{+2} + \text{Ca}^{+2} + \text{SO}_4^{2-} + \text{HCO}_3^-)/\text{Na}^+$ [Holland, 1978]. This approach prevents the inclusion of nss K^+ , Mg^{+2} , Ca^{+2} , SO_4^{2-} , and HCO_3^- in the sea salt mass and allows for the loss of Cl^- through Cl^- depletion processes. It also assumes that all measured Na^+ and Cl^- is derived from seawater.

[15] The overall uncertainty in the ionic mass at the 95% confidence level, propagated as a quadratic sum of all errors, is $\pm 11\%$ for a concentration of 10 $\mu\text{g m}^{-3}$. Details of the uncertainty analysis are provided in the work of Quinn *et al.* [2000a].

2.3. Aerosol Chemical Composition: Organic and Elemental Carbon

[16] Concentrations of OC and EC were not determined for the ACE 1 samples. Details about sampling and analysis for ACE 2 can be found in the work of Novakov *et al.* [2000]. Briefly, a two-stage multijet cascade impactor with 50% aerodynamic cutoff diameters of 1.0 and 10 μm were used for sample collection. Supermicron particles were collected on an Al foil, and submicron particles were collected on a

quartz filter. The impactor also included a second, backup quartz filter to correct for the absorption of gas phase organics. Concentrations of OC and EC were determined by a thermal-evolved gas analysis (EGA) method.

[17] Details of sampling and analysis for OC and EC during Aerosols99 and INDOEX can be found in the work of Quinn *et al.* [2002]. During these experiments, samples were collected with a 3-stage multijet cascade impactor with 50% aerodynamic cutoff diameters of 0.18, 1.0, and 10 μm . Submicron and supermicron samples were collected for the 0.18 to 1.0 μm and 1.0 to 10 μm size range, respectively. All samples were collected on Al foil substrates. A 0.18 μm jet plate was used to minimize positive artifacts due to the absorption of gas phase organics. Samples were analyzed by a thermographic method using a commercial instrument (C-mat 5500, Ströhlein) at the Institute for Tropospheric Research in Leipzig, Germany [Neusüß *et al.*, 2002].

[18] Details of sampling and analysis for OC and EC during ACE Asia and NEAQS can be found in the work of Bates *et al.* [2004]. Single-stage multijet cascade impactors with 50% aerodynamic cutoff diameters of either 1.0 or 10 μm were used for sample collection. Supermicron concentrations were derived from the difference between the two. Denuders were used upstream to avoid absorption of gas phase organics. Concentrations were determined with a Sunset Laboratory, Inc. thermal/optical analyzer [Birch and Cary, 1996].

[19] For all experiments, the mass of particulate organic matter (POM) was determined by multiplying the measured OC concentration in $\mu\text{g m}^{-3}$ by a factor of 1.6. This POM factor is an estimated average of the molecular weight per carbon weight and is based on a review of published measurements of the composition of organic aerosol in urban and nonurban regions [Turpin and Lim, 2001]. On the basis of the range of values given by Turpin and Lim [2001], the POM factor has an uncertainty of $\pm 31\%$.

[20] The uncertainties associated with positive and negative artifacts in the sampling of semivolatile organic species can be substantial [Turpin *et al.*, 1994; Turpin *et al.*, 2000]. No attempt was made to determine the uncertainties associated with these artifacts, since the information to do so was not available. Uncertainty at the 95% level is estimated at ± 24 and 37% , respectively, for modest levels of EC (1.0 $\mu\text{g C cm}^{-2}$) and OC (8.6 $\mu\text{g C cm}^{-2}$).

2.4. Aerosol Chemical Composition: Inorganic Oxidized Material

[21] For Aerosols99, INDOEX, ACE Asia, and NEAQS, total elemental composition (Na, Mg, Al, Si, P, Cl, K, Ca, Ti, V, Cr, Mn, Fe, Ni, Cu, Zn, Ba, As, and Pb) was determined by thin-film X-ray primary and secondary emission spectrometry [Feely *et al.*, 1991; Feely *et al.*, 1998]. Elemental data was not available for ACE 1, ACE 2, and TARFOX. A component composed of inorganic oxidized material (IOM) was constructed from the elemental data by assuming that Al, Si, Ca, Fe, and Ti were present in the aerosol in the most common oxide form [Seinfeld, 1986]. The measured elemental mass concentration was multiplied by the appropriate molar correction factor as follows:

$$[\text{IOM}] = 2.2[\text{Al}] + 2.49[\text{Si}] + 1.63[\text{Ca}] + 2.42[\text{Fe}] + 1.94[\text{Ti}] \quad (2)$$

[Malm *et al.*, 1994; Perry *et al.*, 1997]. This equation includes a 16% correction factor to account for the presence of oxides of other elements such as K, Na, Mn, Mg, and V that are not included in the linear combination. In addition, the equation omits K from biomass burning by using Fe as a surrogate for soil K and average K/Fe ratio of 0.6 in soil [Cahill *et al.*, 1986]. The IOM was most likely composed of soil dust and/or fly ash. The 95% overall uncertainty in the IOM mass, propagated as a quadratic sum of all errors, was $\pm 6\%$ for a concentration of $70 \mu\text{g m}^{-3}$.

2.5. Aerosol Mass

[22] Aerosol mass concentrations were determined by weighing filters before and after sample collection at a humidity of $55 \pm 5\%$. Details of the weighing procedure are found in the work of Quinn and Coffman [1998]. The uncertainty at the 95% confidence level was $\pm 11\%$ for a mass concentration of $20 \mu\text{g m}^{-3}$. Details of chemical composition measurements during TARFOX can be found in the work of Hegg *et al.* [1997] and Novakov *et al.* [1997].

2.6. Aerosol Optical Properties

[23] Measurements of aerosol scattering and hemispheric backscattering coefficients were made with an integrating nephelometer (Model 3563, TSI Inc.) at wavelengths of 450, 550, and 700 nm. The sample RH was measured in the center of the nephelometer sensing volume using a custom-installed capacitive-type RH sensor (Vaisala model HMP135Y). Two single-stage impactors, one with $D_{50,\text{aero}}$ of $1.1 \mu\text{m}$ and one with a $D_{50,\text{aero}}$ of $10 \mu\text{m}$, were placed upstream of the nephelometer. An automated valve switched between the two impactors every 15 min so that sampling alternated between submicron and sub- $10 \mu\text{m}$ aerosol. Values measured by the nephelometer were corrected for an offset determined by measuring filtered air over a period of several hours. In addition, submicron and supermicron values were corrected separately for angular nonidealities of the nephelometer, including truncation errors and nonlambertian illumination, using the method of Anderson and Ogren [1998]. Values are reported at 0°C and 1013 mb. For a 30 min averaging time and a wavelength of 550 nm, a quadrature sum of errors yielded relative uncertainties at the 95% confidence level of $\pm 14\%$.

[24] The absorption coefficient was measured with a Particle Soot Absorption Photometer (PSAP, Radiance Research). The PSAP was downstream of the same impactors as the nephelometer. Measured values were corrected for a scattering artifact, the deposit spot size, the PSAP flow rate, and the manufacturer's calibration as per Bond *et al.* [1999]. Values are reported at a wavelength of 550 nm, 0°C , and 1013 mb. For a 30 min averaging time and an absorption coefficient of 10 Mm^{-1} , a quadrature sum of errors yielded relative uncertainties at the 95% confidence level of $\pm 22\%$.

[25] Aerosol optical depth was derived from observations with a handheld sunphotometer at a wavelength of 500 nm during ACE 1. During ACE 2, AOD was derived from the NASA Ames Research Center's 6-channel Airborne Tracking Sunphotometer (AATS-6) at 525.3 nm [Livingston *et al.*, 2000]. Composite AOD values were derived from all sunphotometers on board the ship during Aerosols99 [Voss *et al.*, 2001], INDOEX [Quinn *et al.*, 2002], and ACE Asia [Quinn *et al.*, 2004]. A handheld Microtops sunphotometer

was used to determine AOD during NEAQS [Quinn *et al.*, 2004]. Details of the measurements of scattering and absorption coefficients and aerosol optical depth during TARFOX can be found in the work of Hegg *et al.* [1997].

2.7. Aerosol Water Content

[26] The chemical thermodynamic equilibrium model AeRho was used to estimate the water mass associated with the inorganic ions at 55% RH. It was assumed that the inorganic aerosol was an internal mixture containing all measured ionic species. The chemical reactions that were allowed to occur, the crystallization humidities used for the solid phase species, and the method for the calculation of the aerosol water content are given in the work of Quinn *et al.* [2002]. Both the IOM and the organic mass were assumed to not take up any water.

2.8. Calculation of Extinction Fractions

[27] AeRho was used to calculate not only aerosol water content but also refractive index and density for each chemical component based on measured size distributions and chemical composition. To check for internal consistency in the measured and modeled parameters, closure experiments were performed for measured and calculated mass and extinction. Details of the calculations and results of the closure experiments have been published for ACE 1 [Quinn *et al.*, 1998; Quinn and Coffman, 1998], Aerosols99 [Quinn *et al.*, 2001], INDOEX [Quinn *et al.*, 2002], and ACE Asia [Quinn *et al.*, 2004]. The procedure for the NEAQS calculations can be found in the work of Quinn *et al.* [2004]. Extinction fractions were not calculated for ACE 2 due to a lack of closure between measured and calculated extinction.

2.9. Air Mass Back Trajectories

[28] Air mass back trajectories were calculated for three arrival heights (500, 2500, and 5500 m) for the ship's position at 6-hour intervals. In cases where a temperature inversion occurred at a sub-500 m height, additional trajectories were calculated for 50 and 100 m arrival heights. Trajectories were calculated with the hybrid single-particle Lagrangian integrated model HY-SPLIT 4 based on the FNL global wind field (available at <http://www.noaa.gov/ready-bin/fnl.pl>) [Draxler, 1992].

3. Results

[29] This paper focuses on the comparison of aerosol plumes downwind of known continental source regions. Calculated air mass back trajectories were used to determine time periods when the sampled air masses had been in contact with the upwind continent ≤ 3 days prior to reaching the ship. Only these time periods were included in the data analysis. The one exception is ACE 1, for which all data are included in order to contrast the remote marine background aerosol to the anthropogenically perturbed aerosol sampled in the other regions. Using this strategy, the regional aerosol that was sampled is labeled according to experiment and aerosol source information. The labels are explained in Table 1.

3.1. Chemical Properties

[30] We first present the average mass fractions of the dominant chemical components for each region. Mass

Table 2. Average Mass Fractions of the Dominant Aerosol Chemical Components for the Submicron ($D_{\text{aero}} < 1.1 \mu\text{m}$), Supermicron ($1.1 < D_{\text{aero}} < 10 \mu\text{m}$), and Sub-10 μm ($D_{\text{aero}} < 10 \mu\text{m}$) Size Ranges^a

Component	ACE 1	ACE 2 Cont	Aer99 Dust	Aer99 Bio Burning	INDOEX Arabia	INDOEX India	ACE Asia Polluted	ACE Asia Poll + Dust	NEAQS Cont
Number of samples	13	16	2	2	2	3	11	7	23
NH ₄ ⁺	0.04 ± 0.01	0.07 ± 0.03	0.04 ± 0.003	0.06 ± 0.01	0.07 ± 0.006	0.09 ± 0.03	0.10 ± 0.01	0.08 ± 0.02	0.05 ± 0.02
nss SO ₄ ²⁻	0.16 ± 0.06	0.46 ± 0.16	0.25 ± 0.02	0.39 ± 0.07	0.30 ± 0.02	0.42 ± 0.08	0.30 ± 0.05	0.26 ± 0.08	0.19 ± 0.08
NO ₃ ⁻	BDL	0.002 ± 0.002	0.03 ± 0.002	0.001 ± 0.0003	0.004 ± 0.001	0.001 ± 0.0004	0.003 ± 0.003	0.01 ± 0.01	0.004 ± 0.003
Sea salt	0.48 ± 0.11	0.02 ± 0.01	0.18 ± 0.01	0.04 ± 0.01	0.03 ± 0.01	0.005 ± 0.002	0.01 ± 0.01	0.01 ± 0.003	0.003 ± 0.002
POM	NA	0.01 ± 0.04	BDL	0.18 ± 0.11	0.15 ± 0.04	0.06 ± 0.01	0.25 ± 0.06	0.18 ± 0.06	0.51 ± 0.14
EC	NA	0.02 ± 0.01	0.01 ± 0.01	0.07 ± 0.01	0.02 ± 0.01	0.07 ± 0.004	0.03 ± 0.01	0.03 ± 0.01	BDL
nss K ⁺	BDL	BDL	0.01 ± 0.0009	0.06 ± 0.01	BDL	0.02 ± 0.0005	BDL	BDL	BDL
IOM (dust)	NA	NA	0.36 ± 0.03	0.05 ± 0.01	0.21 ± 0.06	0.08 ± 0.01	0.05 ± 0.05	0.22 ± 0.15	0.01 ± 0.02
H ₂ O	0.22 ± 0.06	0.24 ± 0.17	0.14 ± 0.02	0.13 ± 0.03	0.21 ± 0.03	0.23 ± 0.02	0.26 ± 0.02	0.21 ± 0.05	0.20 ± 0.08
<i>Submicron</i>									
NH ₄ ⁺	BDL	0.002 ± 0.005	BDL	BDL	BDL	0.001 ± 0.002	0.005 ± 0.004	0.001 ± 0.001	0.004 ± 0.005
nss SO ₄ ²⁻	0.01 ± 0.02	0.03 ± 0.03	BDL	0.005 ± 0.0001	BDL	0.01 ± 0.01	0.02 ± 0.01	0.01 ± 0.02	0.02 ± 0.02
NO ₃ ⁻	BDL	0.16 ± 0.09	0.02 ± 0.001	0.08 ± 0.002	0.05 ± 0.004	0.18 ± 0.06	0.14 ± 0.06	0.04 ± 0.02	0.09 ± 0.05
Sea salt	0.79 ± 0.29	0.47 ± 0.14	0.39 ± 0.01	0.52 ± 0.01	0.28 ± 0.02	0.17 ± 0.07	0.13 ± 0.05	0.07 ± 0.04	0.13 ± 0.06
POM	NA	BDL	0.02 ± 0.002	0.02 ± 0.01	0.01 ± 0.0005	0.08 ± 0.03	0.09 ± 0.06	0.02 ± 0.02	0.21 ± 0.13
EC	NA	BDL	0.0002 ± 0.0002	BDL	0.003 ± 0.001	0.009 ± 0.007	0.01 ± 0.01	0.004 ± 0.003	0.008 ± 0.02
nss K ⁺	BDL	BDL	BDL	0.001 ± 0.001	BDL	0.005 ± 0.001	BDL	BDL	BDL
IOM (dust)	NA	NA	0.41 ± 0.04	0.24 ± 0.03	0.30 ± 0.03	0.30 ± 0.08	0.38 ± 0.16	0.71 ± 0.13	0.22 ± 0.13
H ₂ O	0.20 ± 0.06	0.25 ± 0.16	0.16 ± 0.02	0.13 ± 0.02	0.35 ± 0.03	0.23 ± 0.06	0.21 ± 0.12	0.13 ± 0.07	0.29 ± 0.12
<i>Sub-10 μm</i>									
NH ₄ ⁺	0.01 ± 0.005	0.03 ± 0.02	0.001 ± 0.0001	0.01 ± 0.002	0.01 ± 0.001	0.05 ± 0.02	0.05 ± 0.01	0.02 ± 0.01	0.05 ± 0.02
nss SO ₄ ²⁻	0.03 ± 0.02	0.20 ± 0.10	0.01 ± 0.001	0.08 ± 0.01	0.05 ± 0.005	0.25 ± 0.09	0.15 ± 0.05	0.07 ± 0.03	0.17 ± 0.07
NO ₃ ⁻	BDL	0.08 ± 0.03	0.02 ± 0.001	0.06 ± 0.01	0.04 ± 0.01	0.07 ± 0.02	0.07 ± 0.03	0.03 ± 0.01	0.03 ± 0.01
Sea salt	0.77 ± 0.25	0.30 ± 0.09	0.38 ± 0.03	0.43 ± 0.08	0.25 ± 0.09	0.08 ± 0.07	0.08 ± 0.04	0.06 ± 0.03	0.04 ± 0.03
POM	NA	0.04 ± 0.02	0.02 ± 0.002	0.05 ± 0.04	0.03 ± 0.03	0.06 ± 0.01	0.15 ± 0.06	0.06 ± 0.03	0.33 ± 0.12
EC	NA	0.01 ± 0.004	0.001 ± 0.001	0.02 ± 0.003	0.01 ± 0.005	0.04 ± 0.01	0.02 ± 0.01	0.01 ± 0.005	0.02 ± 0.01
nss K ⁺	BDL	BDL	BDL	0.01 ± 0.003	BDL	0.01 ± 0.004	BDL	BDL	BDL
IOM (dust)	NA	NA	0.40 ± 0.05	0.19 ± 0.04	0.28 ± 0.08	0.17 ± 0.04	0.23 ± 0.13	0.61 ± 0.16	0.08 ± 0.05
H ₂ O	0.21 ± 0.07	0.26 ± 0.15	0.16 ± 0.03	0.13 ± 0.04	0.33 ± 0.05	0.24 ± 0.02	0.24 ± 0.07	0.15 ± 0.06	0.27 ± 0.07

^aStandard deviations (1σ) or uncertainty at the 95% confidence interval (for regions that have ≤ 2 samples) also are given. All measurements are in $\mu\text{g m}^{-3}$. BDL = below detection limit and NA = not available.

fractions indicate how aerosol sources vary regionally, and they help in the interpretation of the fractional contribution each component makes to regional light extinction. Mass fractions do not, however, indicate absolute concentrations, so we also present means and variability of the mass concentrations of the dominant chemical components for each region. In addition, we show mass ratios of the chemical species which yield further information about sources and processing of the chemical components.

3.1.1. Mass Fractions of the Dominant Chemical Components

[31] Regional average mass fractions for the submicron, supermicron, and sub-10 μm size ranges are listed in Table 2 and shown in Figure 2. Average mass fractions for ACE 1 and ACE 2 do not sum to 1 because of a lack of carbon and/or XRF analysis. Until the late 1990s, most model estimates as well as the 1996 Intergovernmental Panel on Climate Change (IPCC) summary of direct aerosol radiative forcing [IPCC, 1996] focused on a highly simplified anthropogenic sulfate-only aerosol. The IPCC Third Assessment Report [IPCC, 2001] was more realistic, with the inclusion of EC, OC, and desert dust. On the basis of the data presented here, nss SO_4^- makes up, on average, 16 to 46% of the submicron aerosol mass at 55% RH. Hence there is a large and variable fraction of the aerosol mass that is not sulfate.

[32] The majority of the submicron mass in the ACE 1 region was sea salt ($48 \pm 11\%$), with nss SO_4^- contributing an additional $16 \pm 6\%$. Sea salt also dominated the supermicron and therefore the sub-10 micron size range with mass fractions of $79 \pm 29\%$ and $77 \pm 25\%$, respectively. The majority of the mass fraction of water in Table 2 and Figure 2 for ACE 1 is associated with sea salt and therefore further enhances the dominance of mass by sea salt.

[33] In regions immediately downwind of continental aerosol sources, the contribution of sea salt to the submicron mass was overwhelmed by contributions from nss SO_4^- , POM, EC, and dust. Sea salt still made a significant contribution to the supermicron mass, however. Further, when the water calculated to be associated with sea salt at 55% RH is taken into account, sea salt made a nonnegligible contribution to the sub-10 micron mass. In all of the continentally influenced regions, nitrate is found in the supermicron rather than the submicron size range, indicating the interaction of HNO_3 and other gas phase oxidized nitrogen species from continental combustion sources with basic sea salt aerosol. The transfer of NO_3^- containing species from submicron to supermicron particles during transport over the oceans may also have contributed to the supermicron nitrate [McGovern *et al.*, 2002].

[34] The contribution of nss SO_4^- and associated NH_4^+ to the submicron mass over all continentally influenced regions averaged 24 to 53% with the highest average mass fractions observed downwind of Europe during ACE 2 and the Indian subcontinent during INDOEX. The POM contribution to the submicron mass was highly variable averaging 1 to 51% over all regions. Highest mass fractions were observed downwind of the NE U.S. during NEAQS Cont. This result is in good agreement with Novakov *et al.* [1997], who reported a mean POM mass fraction of the total dry sub-5 micron aerosol mass of $50 \pm 6\%$ based on an OC to POM conversion factor of $1.7 \mu\text{g POM per } \mu\text{g C}$. Relatively high mass fractions of POM

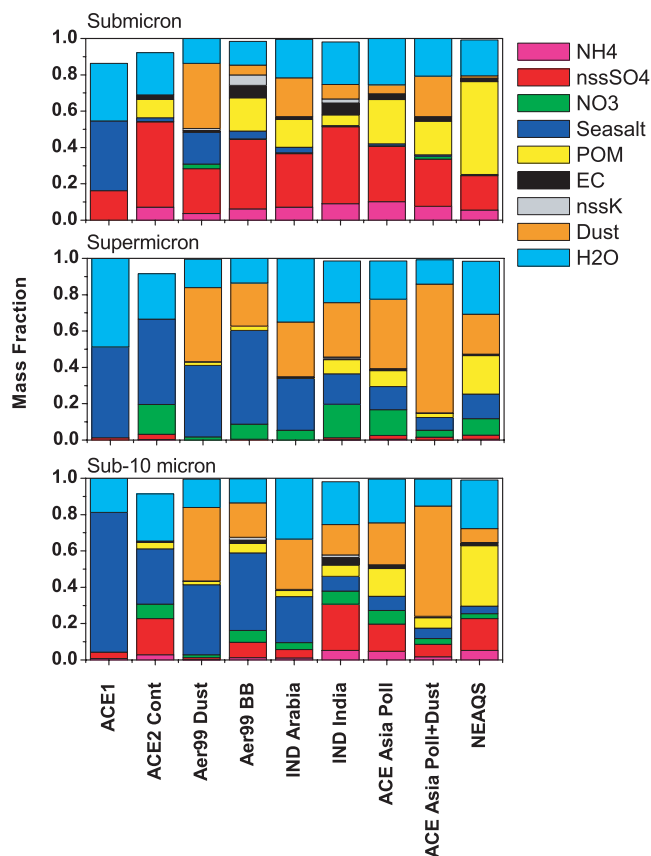


Figure 2. Mean regional mass fractions of the dominant chemical components for the submicron, supermicron, and sub-10 μm size ranges. EC refers to elemental carbon, POM refers to particulate organic matter, and H_2O refers to the amount of water calculated to be associated with the inorganic ionic species at 55% RH.

also were found in the supermicron size range during NEAQS Cont.

[35] Average regional submicron mass fractions of EC ranged from 1 to 7%, with the highest values observed in biomass-burning plumes from Africa (Aerosols99) and downwind of the Indian subcontinent. These two regions also had relatively large (i.e., detectable) submicron mass fractions of nss K^+ , a tracer for biomass burning [e.g., Ferek *et al.*, 1998; Guazzotti *et al.*, 2003].

[36] As mentioned above, sea salt plus associated nitrate was present in the supermicron aerosol in every continentally influenced region studied. The other ubiquitous supermicron chemical component was dust. Supermicron mass fractions of dust were largest during Aerosols99 when the ship encountered air masses that were transported over the dust-producing regions of Africa (Aer99 Dust) and during ACE Asia under conditions of large-scale dust emissions from the Gobi desert region. During Aer99 Dust, IND Arabia, and ACE Asia Poll+Dust, the dust also made a significant contribution to the submicron mass. The sub-10 μm mass fractions shown in Figure 2 for the continentally influenced regions reveal a complex and highly variable mixture of aerosol chemical components, a picture that is far from the sulfate-only aerosol of the early 1990s.

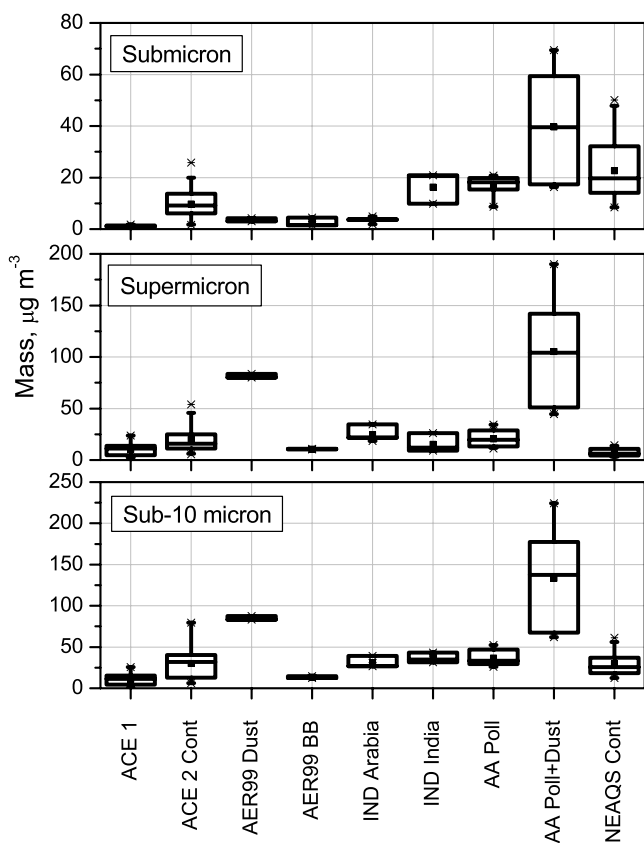


Figure 3. Total aerosols mass concentrations for the submicron, supermicron, and sub-10 micron size ranges. Results are reported at $55 \pm 5\%$ RH. Horizontal lines in the box denote the 25th, 50th, and 75th percentile values. The vertical error bars denote the 5th and 95th percentile values. The two symbols below the 5th percentile bar denote the 0th and 1st percentile and the two symbols above the 95th percentile bar denote the 99th and 100th percentile. The square symbol in the box denotes the mean.

3.1.2. Aerosol Mass Concentrations

[37] Regional mean concentrations and percentile information for aerosol mass are shown in Figure 3 for the submicron, supermicron, and sub-10 μm size ranges. Lowest submicron aerosol mass concentrations were observed during ACE 1, reflecting the distance of the study region from significant continental sources. Relatively low submicron mass concentrations also were measured for the Aer99 Dust, Aer99 BB, and IND Arabia air masses. Back trajectories for the Aer99 Dust and IND Arabia regions indicate that in both cases the sampled air masses had a 2 to 3 day transit in the marine boundary layer from the coast to the ship with patchy cumulus clouds in the Atlantic and clear skies in the Indian Ocean. These conditions suggest that there was little opportunity for aerosol growth between the source region and the ship [Bates *et al.*, 2002]. Back trajectories for the Aer99 BB region indicate that the aerosol sampled on the ship was transported out over the ocean in the free troposphere and mixed down to the MBL in the convective intertropical convergence zone (ITCZ) [Bates *et al.*, 2001]. Hence the aerosol in this air mass experienced a short 2-day transit

over the ocean and dilution by cleaner marine air in the MBL.

[38] ACE 2 submicron mass concentrations covered a relatively wide range (1.8 to $26 \mu\text{g m}^{-3}$) with a mean of $9.7 \pm 5.2 \mu\text{g m}^{-3}$. The variability was a function of the number of source regions sampled (the Mediterranean, the Iberian Coast, and western Europe), the distance from the source to the ship, and the degree of cloud processing [Bates *et al.*, 2000, 2002; Quinn *et al.*, 2000b]. Air masses from the Mediterranean and the Iberian Coast were sampled less than 1 day from the shore and contained aerosol from local point sources along the coast. Number size distributions from both regions were composed of only an Aitken mode with a geometric mean number diameter, D_{gn} , around $0.1 \mu\text{m}$ [Bates *et al.*, 2002]. Particles newly formed from the point sources were quickly depleted through coagulation during the transit to the ship to form the dominant Aitken mode. However, the short transit time did not allow for further growth and the development of an accumulation mode. In contrast, air masses from western Europe sampled off the coast of Portugal had been over the ocean for about 3 days prior to reaching the ship and had one mode in the accumulation mode size range (0.1 to $1 \mu\text{m}$).

[39] Submicron mass concentrations from the IND India region averaged $16 \pm 4.7 \mu\text{g m}^{-3}$. INDOEX took place during the dry winter monsoon season, which is characterized by large-scale subsidence and northeasterly flow from the Indian subcontinent to the northern Indian Ocean. The IND India samples were collected during a period of air mass flow from the Calcutta region to the ship. Submicron mass concentrations from the AA Polluted region were comparable to IND India averaging $16 \pm 3.5 \mu\text{g m}^{-3}$. Air masses in this region had a variety of sources (Japan, Korea, and China) with transit times from the source region to the ship varying from 1 to 2 days for Japan and Korea and several days for China. The average submicron mass concentration for NEAQS Cont was $23 \pm 11 \mu\text{g m}^{-3}$ which is slightly larger than the average for IND India and AA Poll ($\approx 16 \mu\text{g m}^{-3}$).

[40] The lowest average supermicron mass concentration was observed during NEAQS Cont due to the lack of a significant source of either sea salt or dust. Highest average supermicron mass concentrations were observed in the two regions with the highest mass fractions of dust, Aer99 Dust and AA Poll + Dust. A low MBL height contributed to the high supermicron dust and sea salt concentration in the Aer99 Dust region. The overwhelming amount of both submicron and supermicron dust in the AA Poll + Dust region resulted in a sub-10 μm concentration that was much greater than was observed in any other region.

3.1.3. Sea Salt

[41] Sea salt concentrations for the sub- and supermicron size ranges are shown in Figure 4. Average regional submicron concentrations ranged from 0.06 to $0.77 \mu\text{g m}^{-3}$. Average supermicron concentrations were about an order of magnitude higher. Also shown in Figure 4 is the similarity in the trends in local wind speed and sea salt concentration. There are exceptions, however, such as the large supermicron sea salt concentrations in the Aer99 Dust region with no increase in wind speed. Here, the large concentrations are a result of a low and stable MBL. Another exception is the very low sub- and supermicron

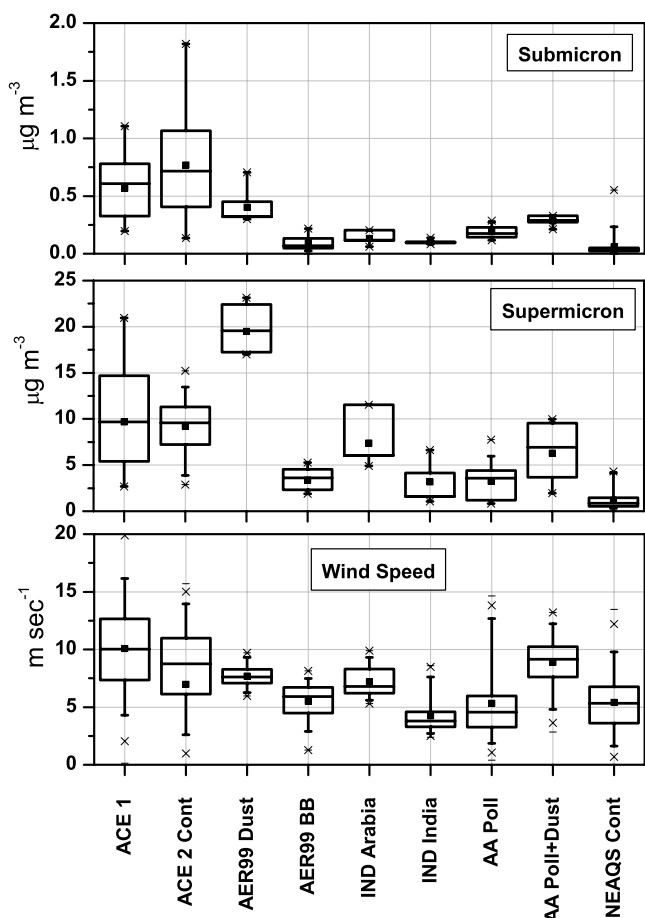


Figure 4. (top and middle) Regional sea salt concentrations for the submicron and supermicron size ranges. True wind speed is shown at the bottom. Percentile information is as described in the Figure 3 caption.

concentrations observed during NEAQS CONT without correspondingly low wind speeds. Hence only a fraction of the variance in the sea salt concentrations can be explained by the local wind speed. Other factors affecting both sub- and supermicron sea salt concentrations include long-range transport, vertical mixing, and dry and wet deposition [Gong *et al.*, 1997; Quinn *et al.*, 1998; Bates *et al.*, 1998a, 1998b].

[42] Sea salt particles that are exposed to H_2SO_4 or HNO_3 typically are depleted in chlorine as the acidic gases react to form Na_2SO_4 or NaNO_3 and release gaseous HCl [Clegg and Brimblecombe, 1985]. In addition, nonacidic gases such as NO_2 , ClNO_3 , and N_2O_5 are thought to react with sea salt to produce gas phase HCl and particulate NaNO_3 [Finlayson-Pitts, 1983; Finlayson-Pitts *et al.*, 1989]. The result of all of these processes is a potentially large loss of particulate chlorine when marine and polluted air masses interact [Keene *et al.*, 1990]. Cl^- to Na^+ mass ratios are shown in Figure 5 as a function of region and particle size along with the seawater mass ratio of 1.8. For both the submicron and supermicron size ranges, the ratio approaches the seawater value for ACE 1 due to the distance of the region from combustion sources. For the continentally impacted regions submicron average values

range from 0.3 to 0.9 and in some instances the ratio is near zero, indicating a complete depletion of chlorine. Supermicron average mass ratios range from 0.65 to 1.9. IND India and AA Polluted, regions with high NO_x emissions have the lowest supermicron ratios. AER99 Dust and AA Poll + Dust have ratios near that of seawater, presumably due to the buffering capacity of the dust.

3.1.4. Non-Sea-Salt Sulfate, OC, and EC

[43] Submicron concentrations of nss SO_4^- plus associated NH_4^+ , OC, and EC are shown in Figure 6. All three chemical components roughly follow the regional trends of submicron aerosol mass. The lowest concentrations of nss SO_4^- plus NH_4^+ were observed in the remote marine region of ACE 1. The ACE 1 mean concentration of $0.17 \pm 0.07 \mu\text{g m}^{-3}$ is on the low end of mean values previously reported for Pacific Ocean latitude bins spanning from 70°S to 60°N (0.28 to $0.58 \mu\text{g m}^{-3}$) [Quinn *et al.*, 2000a]. Relatively low concentrations also were found in the AER99 Dust ($0.65 \pm 0.06 \mu\text{g m}^{-3}$), AER99 BB ($1.0 \pm 0.50 \mu\text{g m}^{-3}$), and IND Arabia ($1.9 \pm 0.12 \mu\text{g m}^{-3}$) regions where transport times and/or pathways and the lack of cloud processing resulted in little aerosol growth. Submicron mean concentrations of $\text{nss SO}_4^- + \text{NH}_4^+$ were fairly similar for the remaining continentally influenced regions ranging from 7 to $13 \mu\text{g m}^{-3}$.

[44] With the exception of one outlier measured during ACE 2, submicron OC was relatively low in the ACE 2

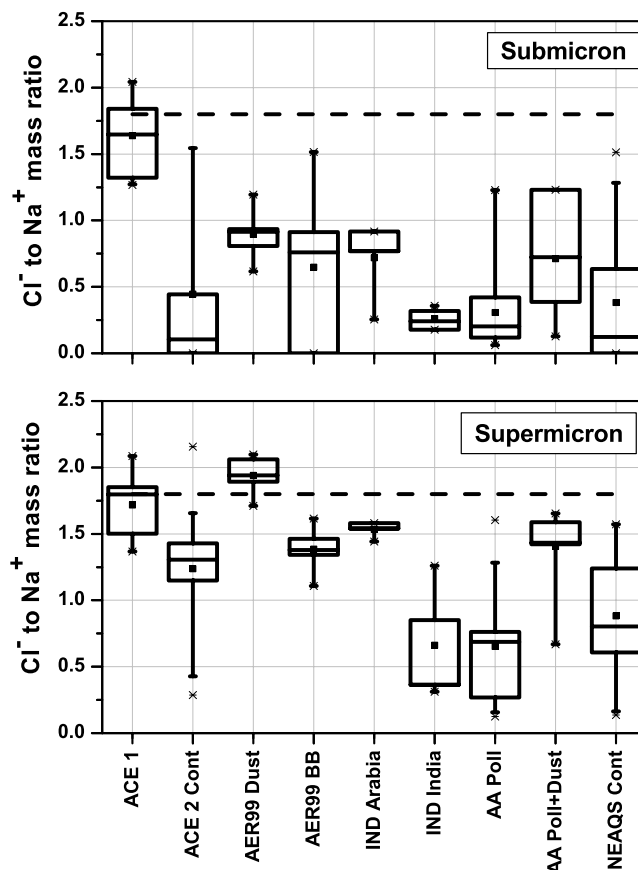


Figure 5. Regional Cl^- to Na^+ mass ratios for the submicron and supermicron size ranges. The dashed line indicates the Cl^- to Na^+ mass ratio for seawater. Percentile information is as described in the Figure 3 caption.

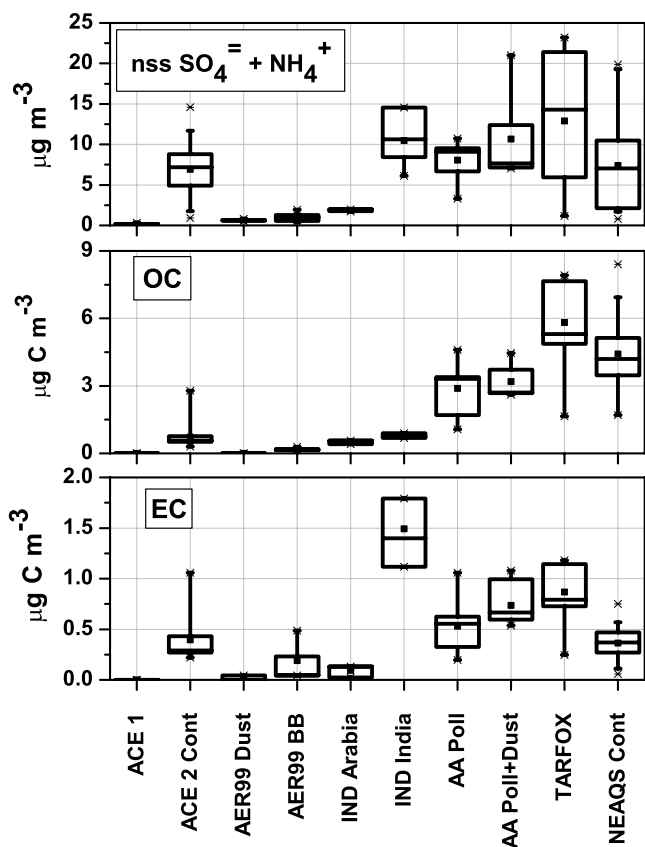


Figure 6. Regional concentrations of $\text{nss SO}_4^- + \text{NH}_4^+$, OC, and EC for the submicron size range. Percentile information is as described in the Figure 3 caption.

Cont, Aer99 Dust, Aer99 BB, and IND Arabia regions with mean values less than $1 \mu\text{g C m}^{-3}$. Higher mean values, ranging from 2.9 to $5.8 \mu\text{g C m}^{-3}$, were measured during AA Poll, AA Poll + Dust, TARFOX, and NEAQS Cont. The TARFOX OC and EC data should be approached with some caution, since the OC values were based on a constant EC to TC ratio of 0.13 [Novakov *et al.*, 1997]. However, the range and mean of the TARFOX concentrations are consistent with the NEAQS Cont measurements, which involved a thermal-optical technique to differentiate EC and OC. The high concentrations and mass fractions of submicron OC in the North American plume also are consistent with ACE 2 observations of a high submicron mass fraction of OC at the Izaña Observatory on Tenerife Island. Putaud *et al.* [2000] hypothesized that the mean OC mass fraction of 64% was due to transport of North American air to Izaña in the free troposphere.

[45] A regional comparison of submicron OC to nss SO_4^- ratios emphasizes the magnitude of OC in the North American plume. For the non-North American air masses, ratios ranged from 0.04 to 0.69 with mean values all less than 0.5. During TARFOX and NEAQS Cont, ratios ranged from 0.27 to 7.6. TARFOX and NEAQS Cont mean ratios were 0.72 ± 0.49 and 1.4 ± 1.3 , respectively. Biogenic precursors such as isoprene and other reactive volatile organic compounds (VOCs) most likely contribute to the elevated OC concentrations observed downwind of the NE United States. On the basis of the NEAQS Cont data set, air

masses from the rural northern U.S. east coast (Maine) had higher OC concentrations and mass fractions than the more urban and industrial regions of the mid-Atlantic (Massachusetts and New York) (T. S. Bates, unpublished data, 2002). Global and regional models estimate that the U.S. isoprene emission rate is larger than that of Germany and Spain by a factor of 30 to 100 [Guenther *et al.*, 1995]. This difference in emissions of natural VOCs could help explain the low OC concentrations measured during ACE 2 downwind of Europe relative to those measured during NEAQS Cont.

[46] Relatively high concentrations of supermicron OC were observed during AA Poll ($1.1 \pm 0.19 \mu\text{g C m}^{-3}$), AA Poll + Dust ($1.8 \pm 0.84 \mu\text{g C m}^{-3}$), and NEAQS Cont ($0.86 \pm 0.44 \mu\text{g C m}^{-3}$), resulting in large supermicron OC mass fractions for these regions. The presence of OC in both the sub- and supermicron size ranges suggests that both gas to particle conversion and condensation of gas phase organics onto existing particles contribute to measured concentrations of particulate OC.

[47] Lowest submicron EC concentrations were observed in the Aer99 Dust and IND Arabia regions, where mean values were less than $0.1 \mu\text{g C m}^{-3}$. Absolute EC concentrations also were low in the Aer99 BB region ($0.19 \pm 0.18 \mu\text{g C m}^{-3}$), but mass fractions were relatively high with a mean of $7 \pm 1\%$. African biomass burning is one of the largest sources of both EC and OC to the global atmosphere [Andreae and Merlet, 2001; Bond *et al.*, 2004] but the concentrations seen in the Aer99 BB air mass were low due to transport through the free troposphere and dilution with remote marine boundary layer air. Comparable EC concentrations were measured during ACE 2 Cont and NEAQS Cont (means of 0.40 ± 0.22 and $0.36 \pm 0.14 \mu\text{g C m}^{-3}$, respectively). Emissions of EC are approximately the same for Europe and North America, with roughly equivalent contributions from transportation, residential combustion, and industry [Cooke *et al.*, 1999; Bond *et al.*, 2004].

[48] Highest EC concentrations were measured downwind of eastern Asia and the Indian subcontinent. Mean submicron concentrations from Ind India, AA Poll, and AA Poll + Dust were 1.5 ± 0.29 , 0.53 ± 0.22 , and $0.74 \pm 0.20 \mu\text{g C m}^{-3}$, respectively. Emissions of EC from China and India result primarily from residential combustion (coal and biofuel in China and biofuel in India) with contributions from industry and transportation. Industrial EC emissions in these regions are heavily influenced by high-emitting technologies (cokemaking and brick kilns) as are transport emissions (two stroke engines). Annual EC emissions from China are estimated to be about a factor of three higher than those of Europe and North America [Bond *et al.*, 2004]. Indian emissions have been estimated to be comparable to those of Europe and North America, although measurements during the INDOEX campaign indicate otherwise. On the basis of measurements of EC and CO downwind of India and estimates of CO emissions in India, Dickerson *et al.* [2002] estimated an EC emission rate 2 to 3 times larger than that of Europe and North America. This analysis does not take into account the different atmospheric loss rates of EC and CO, but it does point out the need to better characterize emissions from Southeast Asia.

[49] Supermicron EC was only observed in detectable quantities (>0.1 up to $1.0 \mu\text{g C m}^{-3}$) in the ACE Asia

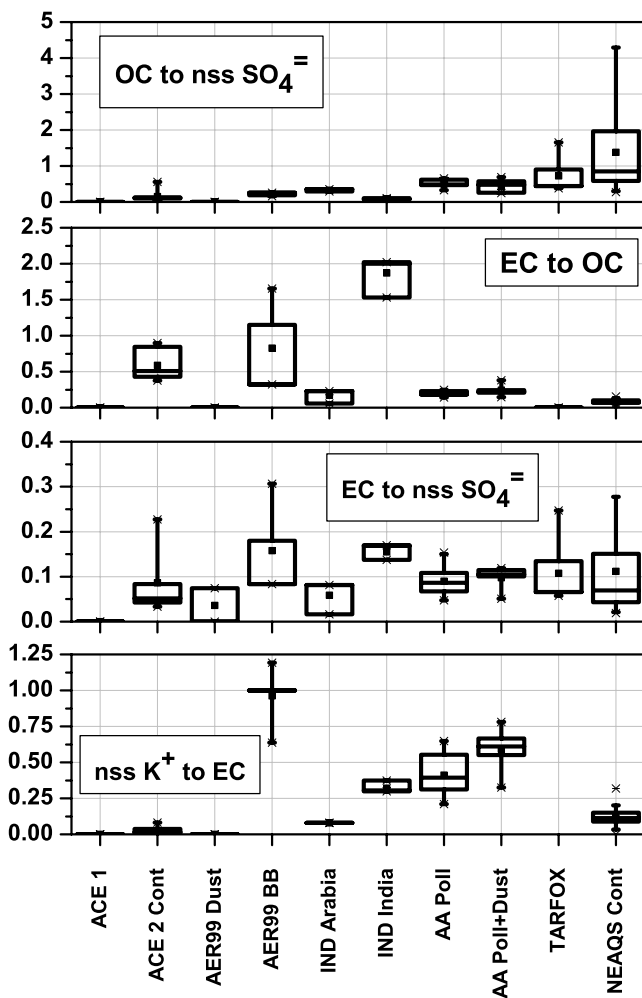


Figure 7. Submicron regional mass ratios of OC to nss SO_4^- , EC to OC, EC to nss SO_4^- , and nss K^+ to EC. Percentile information is as described in the Figure 3 caption.

region. During ACE Asia, concentrations of supermicron EC were highest in the presence of dust, presumably due to the coagulation of soot and dust during transport [Chuang *et al.*, 2003; Quinn *et al.*, 2004].

[50] Reported EC to OC mass ratios due to the combustion of biomass and biofuel fall within the range of 0.07 to 0.3. For example, the reported EC to OC mass ratio for samples of biomass burning in Brazil was 0.12 ± 0.03 [Ferek *et al.*, 1998], for biomass burning in Africa it was 0.22 [Ruellan *et al.*, 1999], and for biofuel burning it was 0.15 ± 0.6 [Andreae and Merlet, 2001]. Higher ratios are expected for fossil fuel emissions. Kleeman *et al.* [2000] reported a ratio near one based on direct measurements of emissions from medium-duty diesel trucks. Urban and industrial emissions from Seoul, Korea and Sapporo, Japan were reported to have EC to OC ratios of 0.76 ± 0.1 [Kim *et al.*, 1999] and 0.97 [Kaneyasu *et al.*, 1995], respectively. These relatively high ratios contrast with those based on 1990 fossil fuel emissions for India. The emission inventory of Reddy and Venkataraman [2002] suggests that the EC to OC mass ratio for fossil fuels used in India ranges from 0.18 to 0.27.

[51] Although the measured submicron EC concentrations for ACE 2 Cont and NEAQS Cont were similar, the NEAQS Cont EC to OC ratio was almost an order of magnitude lower (Figure 7). The mean ACE 2 Cont and NEAQS Cont ratios were 0.59 ± 0.20 and 0.08 ± 0.02 , respectively. The ACE 2 Cont range of values is similar to those expected from fossil fuel burning. The NEAQS Cont very narrow range of low values reflects the large OC concentrations downwind of the NE U.S. The Aer99 Dust EC to OC ratio was below detection limits. Relatively low ratios were observed for the IND Arabia (0.17 ± 0.08), AA Poll (0.19 ± 0.04), and AA Poll+Dust (0.24 ± 0.07) regions (0.08 ± 0.02). These ratios are similar to those expected for biomass and biofuel burning. Highest ratios were observed in the Aer99 BB and IND India regions with mean values of 0.83 ± 0.56 and 1.9 ± 0.22 , respectively. There is a contradiction between the biomass/biofuel source of the EC and OC in these regions and previously reported EC to OC mass ratios for biomass burning.

[52] Non-sea-salt K^+ (nss K^+) is a tracer of biomass/biofuel burning, as it is emitted during most types of biomass burning but not during fossil fuel combustion [Andreae, 1983; Gaudichet *et al.*, 1995]. Reported nss K^+ to EC ratios cover a wide range (0.2 to 1.1), since they are a function of the type of biomass burned [e.g., Andreae *et al.*, 1998; Ferek *et al.*, 1998; Maenhaut *et al.*, 1996]. The low mean submicron nss K^+ to EC mass ratios for ACE 2 Cont (0.02 ± 0.02) and NEAQS CONT (0.11 ± 0.05) are consistent with the interpretation of a fossil fuel source of EC. The relatively low value for IND Arabia (0.08 ± 0.03) indicates a fossil fuel source which contradicts the biomass/biofuel source suggested by the EC to OC ratio. The high mean ratios from Aer99 BB (0.96 ± 0.19), IND India (0.32 ± 0.03), AA Poll (0.41 ± 0.14), and AA Poll + Dust (0.59 ± 0.11) suggest that biomass or biofuel combustion contributed to the measured EC. The high nss K^+ to EC mass ratio for IND India corresponds to high measured concentrations of acetonitrile, a gas phase tracer of biomass/biofuel burning predominantly emitted by smoldering biomass fires [Lobert *et al.*, 1990; Guazzotti *et al.*, 2003]. The conflicting sources of EC (biomass/biofuel versus fossil fuel) based on the EC to OC and nss K^+ to EC mass ratios for the Aer99 BB and IND India regions suggests that (1) emissions of EC and OC from specific sources and regions need better characterization and (2) the effect of atmospheric processing on EC and OC concentrations as pollution aerosol is advected over the ocean needs further study.

3.1.5. IOM

[53] The inorganic oxidized material component was derived from measured trace element concentrations and equation (2). Regional means and variability for the sub- and supermicron size ranges are shown in Figure 8 for seven of the nine regions. IOM concentrations are not available for ACE 1 and ACE 2 because trace elements were not measured. A quick look at Figure 8 reveals the large concentrations of IOM (in this case, dust) measured in the AA Poll + Dust region. The sub- and supermicron mean concentrations in this region were 7.3 ± 5.7 and $75 \pm 33 \mu\text{g m}^{-3}$. Absolute submicron mean concentrations in the other regions were relatively low (ranging from 0.08 to $1.7 \mu\text{g m}^{-3}$). Nonetheless, IOM made up a significant fraction of the mass in the Aer99 Dust and IND Arabia

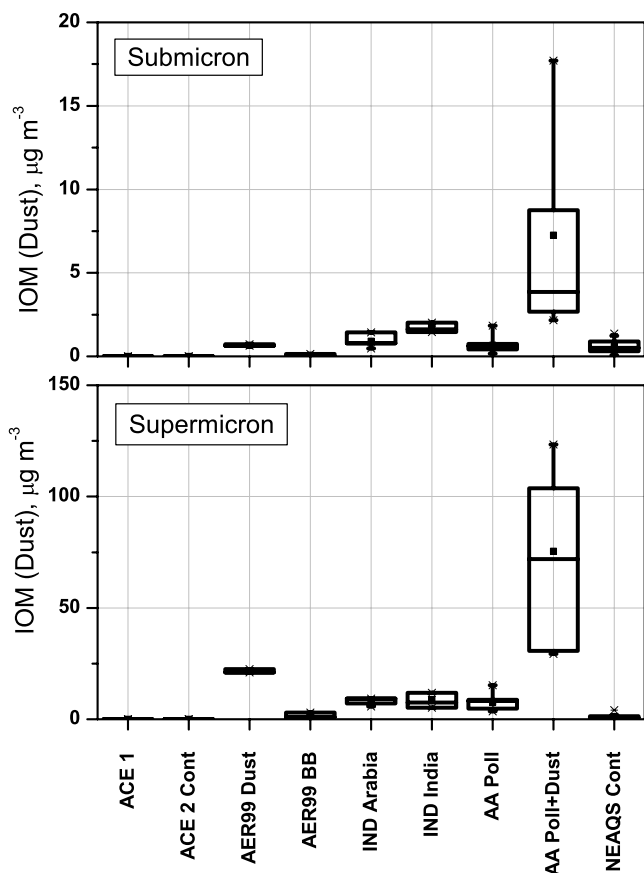


Figure 8. Regional concentrations of Inorganic Oxidized Material (IOM) for the submicron and supermicron size ranges. Percentile information is as described in the Figure 3 caption.

regions (Figure 2). Although absolute supermicron IOM concentrations varied widely between regions (from $0.94 \pm 0.71 \mu\text{g m}^{-3}$ during NEAQS Cont to $22 \pm 0.74 \mu\text{g m}^{-3}$ during Aer99 Dust), it contributed to a significant fraction of the supermicron mass (>20% in all regions).

[54] Si to Al and Fe to Al mass ratios have been reported for aerosol emanating from dust sources around the world. Si to Al ratios from the Sahelian region of Africa range from 3.2 to 3.6 [Bergametti *et al.*, 1989] and from northern Morocco from 2.7 to 2.9 [Bergametti *et al.*, 1989]. The same ratio from central Asia is reported to be around 3.1 [Gomes and Gillette, 1993] and from the northwestern high desert region of China around 2.8 [Alfaro *et al.*, 2003]. In general, then, Si to Al mass ratios for airborne dust from Africa and Asia roughly range from 2.7 to 3.6. Reported Fe to Al mass ratios from the Sahelian region of Africa range from 1.5 to 1.8 [Bergametti *et al.*, 1989], from northern Morocco from 0.7 to 1.1 [Bergametti *et al.*, 1989], and from the northwestern high desert region of China around 0.63 [Alfaro *et al.*, 2003]. Hence Fe to Al mass ratios for airborne dust from Africa and Asia roughly encompass the range of 0.63 to 1.8.

[55] Submicron Si to Al and Fe to Al mass ratios for the seven regions were highly variable both within and between regions. Regional mean values of the submicron Si to Al ratio ranged from 0.3 to 4 and of the Fe to Al ratio from 0.2

to 1.5. Only for the Aer99 Dust region were both Si/Al and Fe/Al consistent with a dust source in the submicron size range. It is likely, then, that industrial sources contributed to the calculated submicron IOM concentrations in the other regions. On the other hand, supermicron Si/Al and Fe/Al ratios for all regions were consistent with dust as the source of calculated IOM concentrations. Figure 9 shows these two mass ratios for the supermicron size range along with lower and upper bounds representing previously reported ratios for African and Asian dust. Mean regional supermicron Si/Al ratios ranged from 2.5 to 3.7 and Fe/Al ratios ranged from 0.56 to 0.95.

3.2. Optical Properties

[56] The directly measured in situ optical properties that are compared include aerosol light scattering, backscattering, and absorption coefficients at 550 nm and $55 \pm 5\%$ RH. In addition, we derive the fine fraction of scattering, FF_{scat} , or the ratio of scattering by the submicron aerosol to scattering by the sub-10 micron aerosol, single-scattering albedo, and aerosol mass scattering efficiency. These aerosol optical properties are strongly dependent on the scattering response of the aerosol to changes in relative humidity. Therefore we use published values of $f(\text{RH})$ to calculate aerosol light scattering, FF_{scat} , and single-scattering albedo at ambient RH. We connect aerosol chemical composition and optical properties by presenting regional mass extinction efficiencies and extinction fractions for the dominant

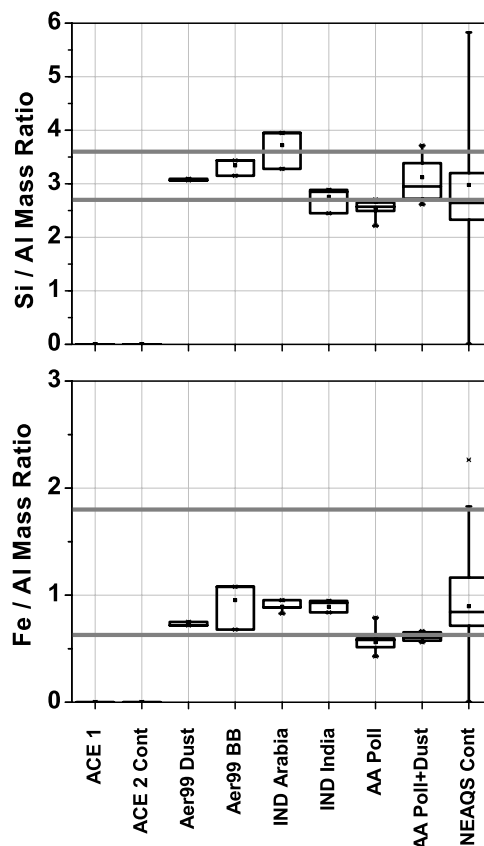


Figure 9. Regional Si to Al and Fe to Al mass ratios for the supermicron size range. Percentile information is as described in the Figure 3 caption.

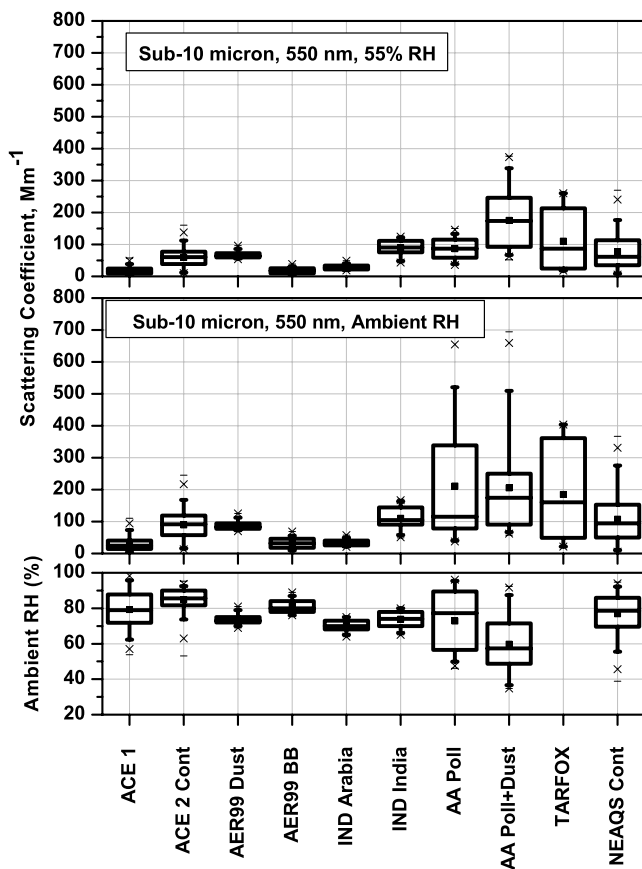


Figure 10. Regional light scattering coefficient for sub-10 micron aerosol at 550 nm. Top box presents data at 55% and the middle data at ambient RH. The latter is based on the information shown in Table 3. Ambient RH for each region also is shown. Percentile information is as described in the Figure 3 caption. Note the TARFOX inlet cut off diameter was most likely less than 10 μm .

chemical components. In addition, we compare the magnitude and variability in aerosol optical depth between regions.

3.2.1. Aerosol Scattering Coefficient

[57] Regional means and variability in sub-10 micron scattering coefficients at 55% and ambient RH are shown in Figure 10. Also shown is the magnitude and variability in ambient RH for all regions. At 55% RH, the regional trends in sub-10 micron scattering follow, for the most part, that of the regional submicron mass concentrations shown in Figure 3. The highest sub-10 micron scattering coefficients were measured in those regions having the highest submicron mass concentrations (ACE 2 Cont, IND India, AA Poll, AA Poll + Dust, and NEAQS Cont). One exception is the Aer99 Dust region, where sub-10 micron scattering was relatively high but the submicron mass was low. Here it is the large supermicron mass composed of dust and sea salt that determined the sub-10 micron scattering. Lowest sub-10 micron scattering was measured during ACE 1 due to its distance from continental source regions and during Aer99 BB where the measured aerosol had been transported through the free troposphere and diluted with marine air as it subsided to the surface.

[58] Sub-10 micron scattering coefficients measured at 55% RH were adjusted to the ambient RH measured during the experiment using the most appropriate estimates of $f(\text{RH})$ available. The source of $f(\text{RH})$ used for each region is listed in Table 3. Regional mean ambient RH scattering coefficients are a factor of 1.2 to 2.5 higher than the 55% RH values. The smallest increases correspond to relatively high mass fractions of dust in both the sub- and supermicron size ranges (Aer99 Dust, IND Arabia, and AA Poll + Dust). The low ambient RH of $58 \pm 14\%$ also contributed to the small increase for AA Poll + Dust. IND India also had a relatively small increase that may have been due to a small sub-10 micron sea salt mass fraction ($8 \pm 7\%$) and a large submicron EC mass fraction of $7 \pm 0.4\%$.

[59] Variability in sub-10 micron scattering for 55% and ambient RH are similar for all regions (as indicated by the 1σ standard deviation divided by the mean value) except for AA Poll and AA Poll + Dust. For these two regions the

Table 3. Source of $f(\text{RH})$ for Conversion of Scattering Coefficients Measured at 55% RH to Scattering Coefficients at Ambient RH

Region	$f(\text{RH})$	Size range	Reference
ACE 1	Curve fit parameters from clean marine conditions at Cape Grim, Tasmania measured during the ACE 1 intensive	Submicron Sub-10 micron	Carrico <i>et al.</i> [1998]
ACE 2 Cont	Curve fit parameters from polluted conditions at Sagres, Portugal measured during the ACE 2 intensive	Submicron Sub-10 micron	Carrico <i>et al.</i> [2000]
Aer99 Dust	$f(\text{RH}) = 1.3$ based on measurements at Barbados when dust composed more than 75% of the aerosol mass	Sub-10 micron	Li-Jones <i>et al.</i> [1998]
Aer99 BB	$f(\text{RH}) = 1.8$ based on measurements during the dry season downwind of S. Africa, Mozambique, and Zambia	Sub-10 micron	Magi and Hobbs [2003]
IND Arabia	Curve fit parameters measured at the Kaashidhoo Observatory for trajectories from Arabia during the INDOEX intensive	Sub-10 micron	A. Jefferson, personal communication, 1999
IND India	Curve fit parameters measured at the Kaashidhoo Observatory for trajectories from the Bay of Bengal during the INDOEX intensive	Sub-10 micron	A. Jefferson, personal communication, 1999
ACE Asia	Curve fit parameters from Polluted and Polluted + Dust time periods measured onboard the ship during ACE Asia	Submicron Sub-10 micron	Carrico <i>et al.</i> [2003]
TARFOX	Curve fit parameters measured onboard the aircraft during TARFOX	Undefined	Kotchenruther <i>et al.</i> [1999]
NEAQS Cont	Curve fit parameters measured at Sable Island, Canada during offshore flow	Sub-10 micron	McInnes <i>et al.</i> [1998]

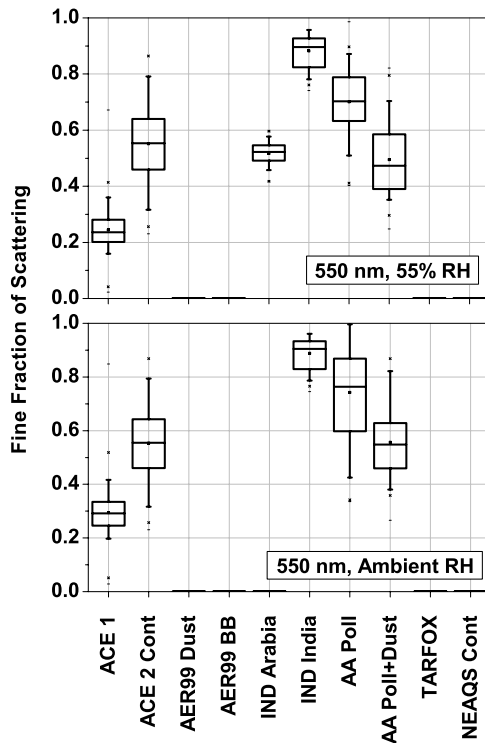


Figure 11. Regional fine fraction of scattering (submicron scattering coefficient divided by the sub-10 micron scattering coefficient). The top shows the ratio at 55% RH and the bottom shows the ratio at ambient RH. Percentile information is as described in the Figure 3 caption.

variability is about a factor of 2 higher for the ambient RH than for 55% RH values. These two regions also have the highest variability in ambient RH.

3.2.2. Fine Fraction of Scattering

[60] *Anderson et al.* [2003] suggested that the FF_{scat} could be used as a categorization scheme to describe variations in aerosol optical parameters. Regional means and variability of FF_{scat} are shown in Figure 11 for both 55% and ambient RH. Values of FF_{scat} were not available for Aer99 Dust, Aer99 BB, and TARFOX, since there were no size-segregated scattering measurements. We also do not report FF_{scat} for NEAQS Cont because the 15-min switching time between the submicron and sub-10 micron size ranges was too slow to capture the variability in scattering as the ship went in and out of plumes.

[61] The lowest values of FF_{scat} at 55% RH were measured during ACE 1 (0.24 ± 0.06) due to the large sea salt coarse mode. Mean values were similar for ACE 2 Cont (0.55 ± 0.14), IND Arabia (0.52 ± 0.04), and AA Poll + Dust (0.49 ± 0.12) but the composition of the coarse mode that dominated sub-10 micron scattering varied between regions. The ACE 2 Cont coarse mode was primarily sea salt. The AA Poll + Dust coarse mode was primarily dust, while the IND Arabia coarse mode was a mixture of sea salt and dust. Hence even though the FF_{scat} was similar for the three regions, the composition and therefore hygroscopicity of the coarse mode was very different.

[62] High FF_{scat} were observed in the IND India region (0.88 ± 0.06) due to a large accumulation mode consisting

primarily of sulfate with smaller amounts of POM and EC. High values also were measured in the AA Poll region (0.70 ± 0.11) due to accumulation mode sulfate and POM with a lesser amount of EC.

[63] FF_{scat} at ambient RH were within 20% of the 55% RH values. This small percent change indicates that depending on region, there was either a similarity in the scattering response of the sub- and supermicron aerosol to changes in RH or ambient RH values were near 55% RH.

[64] The data presented in this paper illustrate how relative amounts of sub- and supermicron aerosol mass affect FF_{scat} . However, they also show how very different sub- and supermicron chemical compositions can yield similar values of FF_{scat} . Hence the ability of the FF_{scat} alone to characterize aerosol optical properties will depend on the mean and variability of the ambient RH, as well as the imaginary refractive index and hygroscopicity of the aerosol components. It may be more appropriate for characterizing the aerosol in a region where the chemical composition is fairly well known than for comparing aerosol properties between several regions.

3.2.3. Backscattered Fraction

[65] The hemispheric backscattered fraction, b , is the scattered intensity that is redirected into the backward hemisphere of the particle. It was derived from the integrating nephelometer measurements and calculated from the ratio of the angular corrected backscattering coefficient (90 to 180°) to the scattering coefficient (0 to 180°). Submicron and sub-10 micron regional means and variability are shown in Figure 12 at 550 nm and 55% RH.

[66] Submicron regional mean values ranged from 0.10 to 0.13 over the seven regions. The sensitivity of top of the atmosphere (TOA) aerosol radiative forcing to changes in b can be estimated from a highly parameterized equation presented by *Haywood and Shine* [1995]. We use the equation here not for accurate estimates of TOA forcing but rather to estimate the sensitivity in the forcing to the range of mean values of b reported here. The equation estimates the global mean, annually averaged TOA forcing due to an optically thin, partially absorbing aerosol. We assume that the daylight fraction is equal to 0.5, fraction of cloud cover is equal to 0.6, and surface albedo is equal to 0.07 and that there is no geographical variation or zenith angle dependence of the parameters used in the equation. In addition, we use the Henyey-Greenstein phase function to calculate the upscatter fraction, β , from b [*Wiscombe and Grams*, 1976; *Sheridan and Ogren*, 1999]. For a constant single-scattering albedo of 0.95 and an aerosol optical depth of 0.3, a change in b from 0.10 to 0.13 results in a change in the aerosol forcing efficiency (forcing per unit aerosol optical depth) from -30 to -34 W m^{-2} , i.e., 4 W m^{-2} .

[67] Mean sub-10 micron values of b covered a wider range from 0.10 to 0.17. The magnitude of b is determined by the size distribution and shape of the particles. It is a complex function of size but, in general, for diameters greater than about 1 micron, b increases with particle size. Model calculations indicate that the scattering phase functions of sharp-edged irregular particles (i.e., dust) are larger than those of volume-equivalent spheres at forward scattering angles ($<10^\circ$) and smaller at backscattering angles ($>150^\circ$) [*Kalashnikova and Sokolik*, 2002]. On the basis purely of shape, then, smaller b values are expected for dust particles.

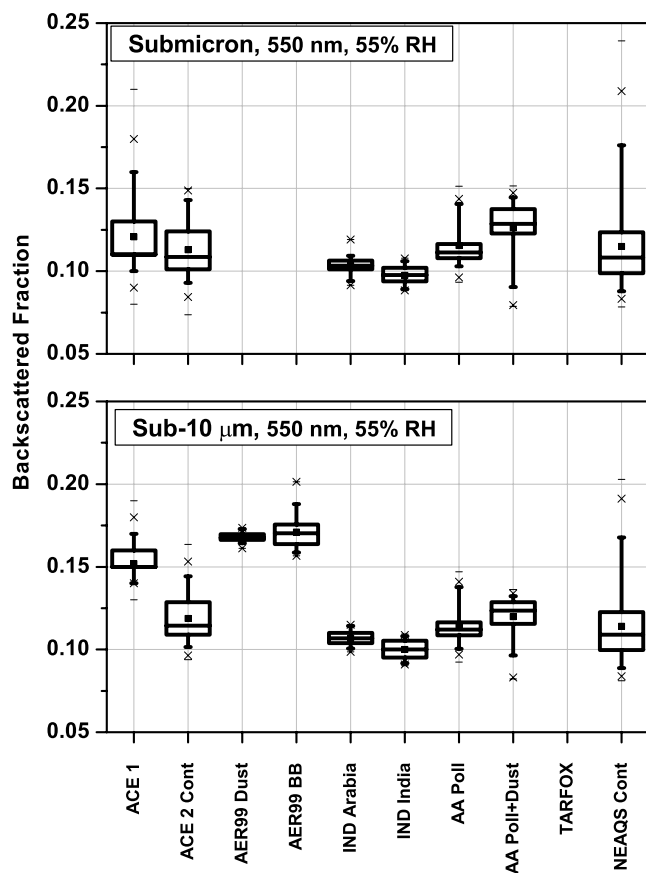


Figure 12. Regional (top) submicron and (bottom) sub-10 micron backscattered fraction at 550 nm and 55% RH. Percentile information is as described in the Figure 3 caption.

[68] Highest values of sub-10 micron b were observed during ACE 1 (0.15 ± 0.01), Aer99 Dust (0.17 ± 0.003), and Aer99 BB (0.17 ± 0.01). For two of these regions (ACE 1 and Aer99 Dust), the ratio of coarse mode to accumulation mode volume was greater than 120 [Bates *et al.*, 2002]. The ratio for Aer99 BB was about 2.3. Hence the relatively large values of b are most likely due to the size distribution of the aerosol in these regions. Mean values of b for the remaining regions ranged from 0.10 to 0.12. The large coarse mode volume during AA Poll + Dust is expected to yield a relatively large b . The expected large value may have been compensated for by the increase in forward scattering due to nonspherical dust particles. Using the method and assumptions outlined above, the sub-10 micron range of b (0.10 to 0.17) results in a change in TOA aerosol forcing efficiency of -30 to -39 W m^{-2} or 9 W m^{-2} .

3.2.4. Absorption Coefficient and Single-Scattering Albedo

[69] Regional means and variability for sub-10 micron absorption coefficients at 55% RH are shown in Figure 13. Lowest values were measured during ACE 1, Aer99 Dust, and IND Arabia where mean values ranged from <0.05 to 1.1 Mm^{-1} . All measurements during Aer99 Dust were below the detection limit (defined as the noise for 30-min averaged data [Bond *et al.*, 1999]). Absorption coefficients for Aer99 Dust were set equal to 0.05 Mm^{-1} , which is the

noise for 30-min averaged data divided by two. Moderate levels of absorption were measured during ACE 2 ($2.7 \pm 2.8 \text{ Mm}^{-1}$), Aer99 BB ($4.7 \pm 3.5 \text{ Mm}^{-1}$), TARFOX ($5.7 \pm 2.5 \text{ Mm}^{-1}$), and NEAQS Cont ($6.0 \pm 3.9 \text{ Mm}^{-1}$). Highest values were measured during IND India ($14 \pm 4.5 \text{ Mm}^{-1}$), AA Poll ($8.8 \pm 3.4 \text{ Mm}^{-1}$), and AA Poll + Dust ($12 \pm 6.3 \text{ Mm}^{-1}$).

[70] There was a measurable contribution to absorption by supermicron aerosol only during ACE Asia [Quinn *et al.*, 2004]. Absorption by supermicron particles made up about 10 and 25% of the absorption for the AA Poll and AA Poll + Dust regions, respectively. On the basis of secondary electron images of individual particles collected on the ship, the supermicron aerosol contained several types of soot, including dust-soot aggregates and solitary black carbon cenospheres (J. Anderson, personal communication, 2001). The dust-soot aggregates appear to result from the coagulation during transport [Huebert *et al.*, 2003]. Carbon cenospheres are hollow balls of black carbon formed by pyrolysis during combustion of heavy fuel oil or coal. This supermicron soot may have contributed to the measured supermicron absorption. However, given the large mass concentrations of dust in this size range, dust is expected to be the major contributor to the supermicron absorption. If the supermicron absorption is subtracted from the sub-10 micron values for ACE Asia, the trends in Figure 13 look very similar to those shown in Figure 6 for submicron EC mass concentrations. Absorption coefficients and submicron EC concentrations were highest downwind of Asia and India, where high EC-emitting technologies are prevalent [Bond *et al.*, 2004].

[71] Single-scattering albedo, defined as the ratio of light scattering by the aerosol to light extinction, is a measure of the absorptivity of the aerosol with lower values indicating a more absorbing aerosol. We show the sensitivity of SSA to particle size in Figure 14 for a wavelength of 550 nm and a relative humidity of 55%. Regional mean values of submi-

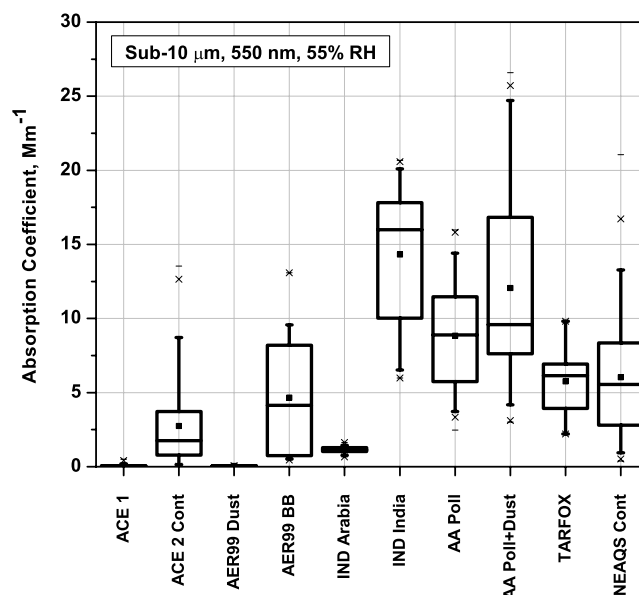


Figure 13. Regional sub-10 micron absorption coefficient at 550 nm and 55% RH. Percentile information is as described in the Figure 3 caption.

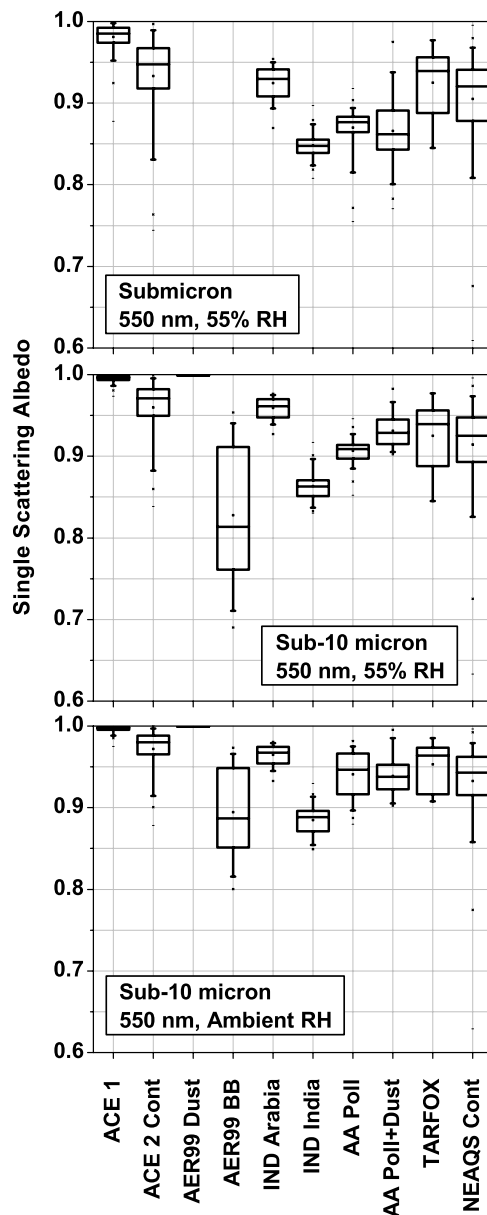


Figure 14. Regional single-scattering albedo for the (top) submicron and (middle) sub-10 micron size ranges at 55%. Also shown is (bottom) sub-10 micron single-scattering albedo at ambient RH. All values are reported at 550 nm. Percentile information is as described in the Figure 3 caption. TARFOX values are the same for the submicron and sub-10 micron size ranges since the inlet cutoff diameter was not reported.

cron SSA at 55% RH ranged from 0.98 for ACE 1 (where the aerosol was essentially completely reflective with no absorptive mass) to 0.85 for IND India (where EC made up 7 ± 0.4 % of the submicron mass). The three regions with high levels of absorption and submicron EC concentrations had the lowest submicron SSA (IND India (0.85 ± 0.01), AA Poll (0.87 ± 0.02), and AA Poll + Dust (0.87 ± 0.04)). The other regions where submicron data were available had mean values between 0.90 and 0.93 (ACE 2 Cont, IND Arabia, TARFOX, and NEAQS Cont).

[72] Regional mean sub-10 micron values of SSA at 55% RH were 1 to 8% higher than their submicron counterparts. There was little difference ($\leq 3\%$) for regions where both the sub- and supermicron aerosol were primarily composed of reflective and not absorptive components (ACE 1 and ACE 2 Cont) or where the submicron aerosol mass concentration was much larger than the supermicron concentration (NEAQS Cont). The small difference for the IND India region (2%) may be a result of a significant mass fraction of a hydrophobic species in both the submicron (EC) and supermicron (dust) size ranges. It may also be due to the use of $f(\text{RH})$ values from KCO rather than the ship with the latter presumably sampling aerosol with a larger sea salt mass fraction. Larger differences between submicron and sub-10 micron SSA at 55% RH were observed for regions where the supermicron mass concentration was a factor of 2 or more greater than the submicron mass concentration and/or the supermicron aerosol was composed of a large fraction ($\geq 38\%$) of dust (IND Arabia, AA Poll, AA Poll + Dust). In the AA Poll + Dust region the supermicron EC and resulting absorption did not lead to relatively low sub-10 micron values of SSA due to the overwhelming concentration of dust. The sub-10 micron SSA measured on the ship for this region (0.93 ± 0.02) was similar to that measured on board the aircraft in relatively unpolluted dust layers in the free troposphere (0.95 ± 0.02) [Anderson *et al.*, 2003].

[73] The sensitivity of SSA to changes in scattering due to changes in RH also is shown in Figure 14. Sub-10 micron SSA was calculated at ambient RH using the scattering coefficient adjusted to ambient RH (Table 2) and the absorption coefficient at 55% RH. We did not attempt to adjust absorption coefficients to ambient RH because the information required to do so is currently not available. The magnitude of the difference between 55% and ambient RH sub-10 micron SSA is a function of the hygroscopicity of the aerosol and how far above 55% the ambient RH is. Mean differences over all regions ranged from 0 to 8%. There was no significant difference for regions composed of primarily scattering components. For example, for ACE 1 and Aer99 Dust, the 55% RH SSA was nearly at the maximum of 1. In this case an increase in scattering level due to hygroscopic growth does not impact SSA. Two regions that exhibited a 1% increase had relatively low ambient RH (IND Arabia ($70 \pm 3\%$) and AA Poll + Dust ($58 \pm 14\%$)). The increase in SSA for ACE 2 Cont, IND India, AA Poll, and NEAQS Cont ranged from 1 to 4%. The largest difference was seen for the Aer99 BB region where there was a large sub-10 micron mass fraction of hygroscopic sea salt and a mass fraction of submicron EC of 7% contributing to absorption.

[74] Using the method and assumptions described in section 3.2.3, we calculated the sensitivity of the TOA aerosol forcing efficiency to the range of regional mean SSA presented here. For these calculations, we assumed a backscattered fraction of 0.12 and AOD of 0.3. For SSA ranging from 0.85 to 0.99, we calculated TOA aerosol forcing efficiencies ranging from -27 to -35 W m^{-2} or a change of 8 W m^{-2} . Solar radiation flux measurements from space and the surface during INDOEX revealed that the haze-induced reduction in surface solar radiation was three times larger than the reflected solar radiation at the top of the

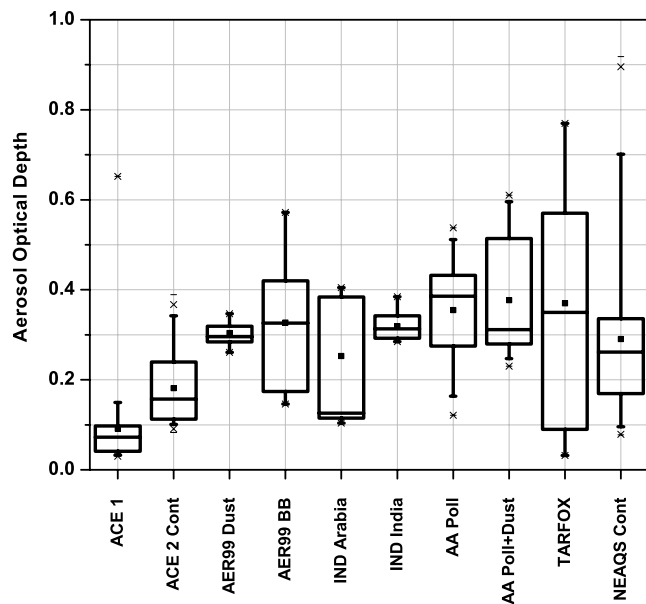


Figure 15. Regional aerosol optical depth. All values are reported at 500 nm except those for ACE 2 (525.3 nm) and TARFOX (405 nm). Percentile information is as described in the Figure 3 caption.

atmosphere for clear skies [Satheesh and Ramanathan, 2000]. Hence the absorption by EC in the IND India region had a larger impact on surface than TOA forcing. The hydrological impacts of this reduction in solar radiation to the surface have been hypothesized to be significant but currently are not well understood [Ramanathan and Crutzen, 2003]. Solar heating of the boundary layer by EC also may lead to evaporation of some clouds which would result in more solar radiation reaching the surface and a subsequent warming of the surface [Ackerman *et al.*, 2000].

3.2.5. Aerosol Optical Depth

[75] Regional means and variability in AOD are shown in Figure 15. The low values observed during ACE 1 (0.09 ± 1.1) are typical of remote marine regions [Smirnov *et al.*, 2002]. The continental regional mean values ranged from a low of 0.18 for ACE 2 Cont to 0.38 for AA Poll + Dust. With the exception of ACE 2 Cont, the continental regional means were remarkably consistent ranging from 0.25 to 0.38. This result is in contrast to the nephelometer-measured sub-10 micron scattering where Aer99 Dust, Aer99 BB, and IND Arabia had low mean values compared with the other continental regions. On the basis of shipboard lidar measurements during Aer99 and INDOEX, the reason for the difference between surface-measured scattering and AOD is the presence of aerosol layers aloft [Voss *et al.*, 2001; Welton *et al.*, 2002].

3.2.6. Aerosol Mass Scattering Efficiency

[76] Mass scattering efficiencies (MSE) for the total aerosol were calculated from the measured light-scattering coefficient divided by the measured aerosol mass concentration. Light-scattering coefficients were averaged over the time period that the mass samples were collected. MSE were calculated for the submicron and sub-10 micron size ranges. Values are reported at 55% RH, since this was the measurement RH for both scattering and mass (Figure 16).

[77] Regional mean submicron values are consistent for all regions ranging from 3.2 to $4.1 \text{ m}^2 \text{ g}^{-1}$. The variability, as measured by the 1σ standard deviation divided by the mean, is similar for all ranging from -0.06 to 0.09 . On the basis of these results, variability in the shape (accumulation mode mean diameter and width) of the aerosol size distribution is not large enough to lead to large differences in submicron MSE. For ACE 2 Cont, IND Arabia, and IND India, mean accumulation mode geometric mean diameters range from 0.35 to $0.39 \mu\text{m}$, while the remote marine value for ACE 1 is $0.19 \mu\text{m}$ [Bates *et al.*, 2002]. Modal parameters are not yet available for ACE Asia or NEAQS.

[78] Mean sub-10 micron MSE are not as uniform as their submicron counterparts ranging from 0.78 to $3 \text{ m}^2 \text{ g}^{-1}$. Higher values were found in regions where the submicron to sub-10 micron mass ratio was greater than 30% (ACE 2 Cont, IND India, AA Poll, and NEAQS Cont). NEAQS Cont had the highest mean sub-10 micron MSE ($3 \pm 0.6 \text{ m}^2 \text{ g}^{-1}$) and the highest submicron to total mass ratio of 76%. This result indicates that sub-10 micron MSE are controlled by the relative magnitudes of the accumulation and coarse mode aerosol.

3.2.7. Aerosol Mass Absorption Efficiency

[79] Mass absorption efficiencies (MAE) for sub-10 micron aerosol were calculated from the measured light absorption coefficient divided by the measured EC con-

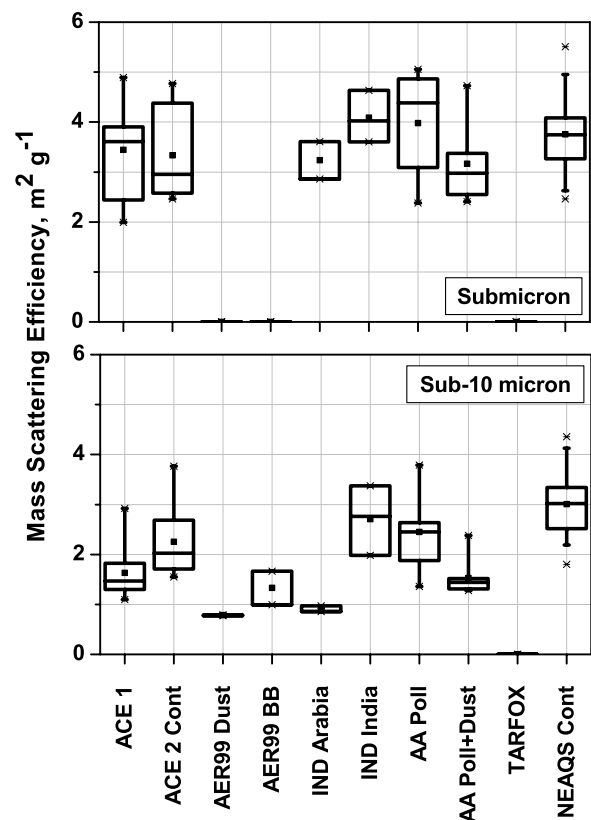


Figure 16. Regional mass scattering efficiencies for the (top) submicron and (bottom) sub-10 micron size ranges. Mass scattering efficiency is defined as the light scattering by the aerosol at 550 nm and 55% RH per unit mass. Percentile information is as described in the Figure 3 caption.

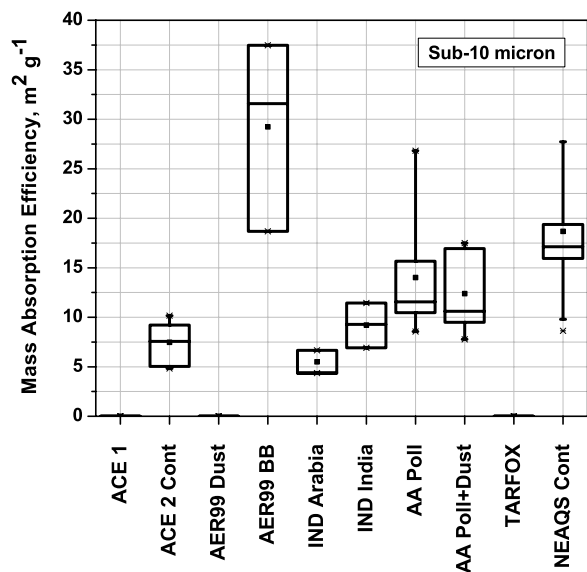


Figure 17. Regional mass absorption efficiencies for the sub-10 micron size range at 550 nm and 55% RH. Mass absorption efficiency is defined as the light absorption by the aerosol divided by the EC mass concentration. Percentile information is as described in the Figure 3 caption.

centration. Light absorption coefficients were averaged over the time period that the EC samples were collected. For most regions, absorption and EC were confined primarily to the submicron size range so the sub-10 micron MAE is equivalent to the submicron size range. Values are reported at 55% RH (Figure 17).

[80] Regional mean values ranged from 5.5 to 39 $\text{m}^2 \text{g}^{-1}$. Mass absorption efficiency defined as the absorption coefficient of EC divided by the mass of EC has a theoretical limit of 10 $\text{m}^2 \text{g}^{-1}$ if it is calculated from Mie theory at 550 nm with commonly assumed densities and refractive indices of EC [e.g., Martins *et al.*, 1998; Fuller *et al.*, 1999]. Values reported here rise above this theoretical limit. It may be that the assumption of internally mixed homogeneous single spheres of EC, as required by Mie theory, does not accurately describe all regional aerosol mixtures. Fuller *et al.* [1999] extended Mie theory beyond single carbon spheres and showed that MAE can exceed 10 $\text{m}^2 \text{g}^{-1}$ by a factor of 2.5 to 4 for carbon spheres embedded in host particles having a refractive index between 1.33 and 1.53 and a diameter greater than 0.4 μm .

[81] Alternatively, if the aerosol is well described by Mie theory, it may indicate instrumental issues including (1) the thermo-optical technique does not accurately measure all midvisible absorbing species present, (2) the difficulty in accurately determining the split point between OC and EC in the thermo-optical analysis, and/or (3) the inability to parameterize the PSAP scattering correction factor under certain conditions (e.g., large dust loadings on the filter) and the uncertainty in the transmission function.

3.2.8. Aerosol Component Mass Extinction Efficiencies

[82] Mass extinction efficiencies of the individual chemical components are defined as

$$\text{MEE}_j = \sigma_{\text{ep},j} / m_j, \quad (3)$$

where $\sigma_{\text{ep},j}$ is the light extinction due to component j and m_j is the mass concentration of component j . The MEE of a chemical component is essential for estimating its direct radiative forcing. MEE_j ($\text{m}^2 \text{g}^{-1}$) were estimated from component extinction calculated with a Mie model and measured mass concentrations of the chemical components. Details of the Mie calculations can be found in the references listed in Table 4. Average and 1σ standard deviations of regional MEE_j are reported in Table 4 at 550 nm and 55% RH. The components include sea salt (which includes supermicron NO_3^- and associated H_2O), nss sulfate aerosol (which includes nss SO_4^{2-} , NH_4^+ , and associated H_2O), IOM or dust, POM (derived from OC assuming an OC to POM factor of 1.6), and EC (which includes submicron nss K^+ with associated nss SO_4^{2-} and NO_3^-). The IOM, POM, and EC components were assumed to be hydrophobic.

[83] Submicron sea salt MEE tend to be slightly larger than the submicron nss sulfate aerosol values. This result indicates the importance of including size segregated sea salt in estimates of aerosol direct radiative effects for regions where submicron sea salt concentrations are equal to or greater than the nss sulfate concentrations.

[84] In general, MEE for a component within a given size range are consistent between regions. The one exception to this is POM where mean supermicron values range from 1.1 to 5.5 $\text{m}^2 \text{g}^{-1}$. The wide range of values could be due to differences in organic composition, size distribution, and/or sampling methods.

[85] The effect of assuming that IOM and POM do not take up any water is difficult to quantify. Liousse *et al.* [1996] assumed that the water uptake by POM was similar to that of sulfate aerosol and estimated that MEE_{POM} increased from 4 $\text{m}^2 \text{g}^{-1}$ for a dry aerosol to 6.8 $\text{m}^2 \text{g}^{-1}$ for an aerosol at 80% RH due to an increase in particle size. The competing effect of lowering the refractive index must also be considered, however. The uptake of water by dust and POM is an uncertainty that must be addressed to improve the accuracy of forcing calculations.

3.2.9. Extinction Fractions of the Dominant Chemical Components

[86] The fraction of the measured light extinction due to the dominant chemical components was calculated at 55% RH and 550 nm using a Mie model and measured number size distributions and size-segregated chemical mass concentrations. Details of the calculations can be found in the references listed in Table 5. Only the inorganic ion components (sea salt and nss sulfate) were assumed to take up water. The major components considered were the same as those listed in section 3.2.7. Results are shown for the submicron, supermicron, and sub-10 micron size ranges in Figure 18 and Table 5.

[87] In general, the trend in extinction fraction for each chemical component follows the trend in their mass fraction shown in Figure 2. In the remote marine region of ACE 1, sea salt dominates extinction in all size ranges. This Southern Ocean result confirms earlier findings from the central Pacific Ocean that sea salt dominates aerosol extinction in all size ranges in the remote marine atmosphere [Quinn and Coffman, 1999] and indicates the need to consider both submicron and supermicron sea salt when estimating the radiative effects of marine aerosols. In

Table 4. Mean and Standard Deviation of the Mass Extinction Efficiencies of the Major Chemical Components in Each Region Based on Mie Calculations at 550 nm and 55% RH

Region	Sea salt ^a	Nss SO ₄ ⁻ aerosol ^b	IOM (dust) ^c	POM ^d	EC ^e	Reference
<i>Submicron</i>						
ACE 1	4.5 ± 1.1	1.3 ± 0.55	NA	NA	NA	<i>Quinn and Coffman</i> [1999]
ACE 2 Cont ^f	3.1 ± 3.7	3.6 ± 0.77	NA	NA	NA	P. K. Quinn, unpublished data, 2002
Aer99 Dust	5.9 ± 1.0	2.6 ± 0.5	3.5 ± 0.6	7.1 ± 1.0	3.2 ± 0.5	<i>Quinn et al.</i> [2001]
Aer99 BB	6.6 ± 1.5	4.3 ± 0.9	4.5 ± 0.9	6.9 ± 1.4	5.7 ± 1.1	<i>Quinn et al.</i> [2001]
IND Arabia	5.3 ± 1.1	3.2 ± 0.4	3.1 ± 0.6	5.4 ± 0.8	4.7 ± 0.1	<i>Quinn et al.</i> [2002]
IND India	5.7 ± 0.1	5.3 ± 0.1	4.3 ± 0.1	7.6 ± 0.1	5.8 ± 0.01	<i>Quinn et al.</i> [2002]
AA Poll	4.6 ± 0.68	3.7 ± 0.42	3.2 ± 0.32	5.4 ± 0.33	3.9 ± 0.12 ^g	<i>Quinn et al.</i> [2004]
AA Poll + Dust	5.4 ± 1.5	3.6 ± 0.27	3.5 ± 0.26	5.0 ± 0.37	3.9 ± 0.32 ^g	<i>Quinn et al.</i> [2004]
NEAQS Cont	6.6 ± 1.1	4.3 ± 0.77	3.0 ± 1.1	4.7 ± 1.5	5.7 ± 3.0	<i>Quinn et al.</i> [2004]
<i>Supermicron</i>						
ACE 1	1.2 ± 0.18	NA	NA	NA	NA	<i>Quinn and Coffman</i> [1999]
ACE 2 Cont ^f	2.8 ± 0.44	NA	NA	NA	NA	P. K. Quinn, unpublished data, 2002
Aer99 Dust	1.2 ± 0.2	NA	0.5 ± 0.1	1.1 ± 0.1	NA	<i>Quinn et al.</i> [2001]
Aer99 BB	1.2 ± 0.4	NA	0.6 ± 0.2	2.1 ± 0.5	NA	<i>Quinn et al.</i> [2001]
IND Arabia	1.0 ± 0.3	4.3 ± 1.9	0.5 ± 0.2	3.8 ± 0.6	NA	<i>Quinn et al.</i> [2002]
IND India	1.0 ± 0.1	2.9 ± 0.1	0.6 ± 0.1	5.5 ± 0.1	NA	<i>Quinn et al.</i> [2002]
AA Poll	1.4 ± 0.15	2.3 ± 0.62	0.47 ± 0.05	1.9 ± 0.77	NA	<i>Quinn et al.</i> [2004]
AA Poll + Dust	1.7 ± 0.12	3.6 ± 0.78	0.75 ± 0.11	2.1 ± 0.76	NA	<i>Quinn et al.</i> [2004]
NEAQS Cont	1.3 ± 0.63	6.1 ± 3.8	0.69 ± 0.46	2.4 ± 1.5	NA	<i>Quinn et al.</i> [2004]

^aIncludes NO₃⁻ and H₂O at 55% RH.^bIncludes nss SO₄⁻, NH₄⁺, and H₂O at 55% RH.^cDoes not include H₂O.^dBased on a conversion factor of μg POM per μg of C of 1.6. Does not include H₂O.^eIncludes nss K⁺ with associated nss SO₄⁻ and NO₃⁻ to form a “burning component.”^fBased on a multiple linear regression of measured scattering and measured sulfate and sea salt aerosol concentrations.^gMass scattering efficiency, not mass absorption efficiency.

addition, in six of the seven continental regions shown in Figure 18, sea salt makes a significant contribution to extinction in all size ranges due to its propensity to take up and hold onto water. As RH decreases from 70 to 55%, sea salt retains water such that the wet particle mass is twice its dry mass [*Tang et al.*, 1997].

[88] For the continental regions, total extinction is a result of a complex and highly variable mixture of chemical

components for all size ranges. Scattering by nss SO₄⁻ and the resulting radiative forcing have been the subject of much study. By comparison, the impacts of dust, POM, and EC on climate are not as well characterized for a variety of reasons. Each of these components is not a single chemical species but rather a “category” into which a multitude of species are collected. Dust species and aggregates of species vary chemically and morphologically

Table 5. Average Extinction Fractions of the Dominant Aerosol Chemical Components for the Submicron ($D_{\text{aero}} < 1.1 \mu\text{m}$), Supermicron ($1.1 < D_{\text{aero}} < 10 \mu\text{m}$), and Sub-10 μm ($D_{\text{aero}} < 10 \mu\text{m}$) Size Ranges^a

Component	ACE 1	Aer99 Dust	Aer99 Bio Burning	INDOEX Arabia	INDOEX India	ACE Asia Polluted	ACE Asia Poll + Dust	NEAQS Cont
<i>Submicron</i>								
Number of samples	13	2	2	2	3	11	7	23
nss SO ₄ ⁻ + NH ₄ ⁺	0.09 ± 0.07	0.11 ± 0.04	0.34 ± 0.16	0.31 ± 0.08	0.44 ± 0.08	0.39 ± 0.08	0.34 ± 0.11	0.33 ± 0.19
Sea salt	0.89 ± 0.07	0.62 ± 0.19	0.30 ± 0.13	0.20 ± 0.06	0.04 ± 0.06	0.26 ± 0.07	0.21 ± 0.16	0.07 ± 0.05
POM	NA	0.01 ± 0.004	0.20 ± 0.10	0.23 ± 0.06	0.12 ± 0.06	0.22 ± 0.05	0.16 ± 0.05	0.54 ± 0.20
EC	NA	0.01 ± 0.004	0.06 ± 0.03	0.08 ± 0.02	0.35 ± 0.02	0.05 ± 0.05	0.05 ± 0.02	0.02 ± 0.03
IOM (dust)	NA	0.24 ± 0.08	0.09 ± 0.04	0.18 ± 0.05	0.05 ± 0.05	0.09 ± 0.07	0.24 ± 0.10	0.03 ± 0.05
<i>Supermicron</i>								
nss SO ₄ ⁻ + NH ₄ ⁺	BDL	0.001 ± 0.0003	0.02 ± 0.01	0.02 ± 0.01	0.08 ± 0.01	0.08 ± 0.05	0.07 ± 0.03	0.11 ± 0.13
Sea salt + NO ₃ ⁻	100	0.79 ± 0.18	0.85 ± 0.42	0.74 ± 0.43	0.54 ± 0.43	0.56 ± 0.11	0.25 ± 0.10	0.45 ± 0.19
POM	NA	0.02 ± 0.004	0.05 ± 0.02	0.06 ± 0.03	0.22 ± 0.03	0.12 ± 0.07	0.05 ± 0.04	0.36 ± 0.20
EC	NA	0.0003 ± 0.0001	0.002 ± 0.001	0.01 ± 0.001	0.06 ± 0.01	0.02 ± 0.02	0.01 ± 0.006	0.007 ± 0.01
IOM (dust)	NA	0.19 ± 0.04	0.07 ± 0.05	0.18 ± 0.11	0.10 ± 0.11	0.22 ± 0.08	0.62 ± 0.10	0.07 ± 0.09
<i>Sub-10 micron</i>								
nss SO ₄ ⁻ + NH ₄ ⁺	0.04 ± 0.04	0.02 ± 0.006	0.20 ± 0.09	0.18 ± 0.06	0.42 ± 0.06	0.30 ± 0.07	0.23 ± 0.12	0.30 ± 0.18
Sea salt + NO ₃ ^{-b}	0.96 ± 0.04	0.76 ± 0.20	0.54 ± 0.24	0.45 ± 0.17	0.07 ± 0.17	0.34 ± 0.04	0.22 ± 0.14	0.13 ± 0.09
POM	NA	0.02 ± 0.004	0.14 ± 0.06	0.15 ± 0.05	0.13 ± 0.05	0.19 ± 0.05	0.11 ± 0.06	0.51 ± 0.19
EC	NA	0.003 ± 0.001	0.04 ± 0.02	0.05 ± 0.02	0.33 ± 0.02	0.04 ± 0.01	0.04 ± 0.02	0.02 ± 0.03
IOM (dust)	NA	0.20 ± 0.05	0.09 ± 0.04	0.18 ± 0.07	0.06 ± 0.07	0.13 ± 0.08	0.40 ± 0.13	0.04 ± 0.06

^aStandard deviation or uncertainty at the 95% confidence interval (for regions that have ≤2 samples) also are given. NA = not available.^bSupermicron NO₃⁻ only.

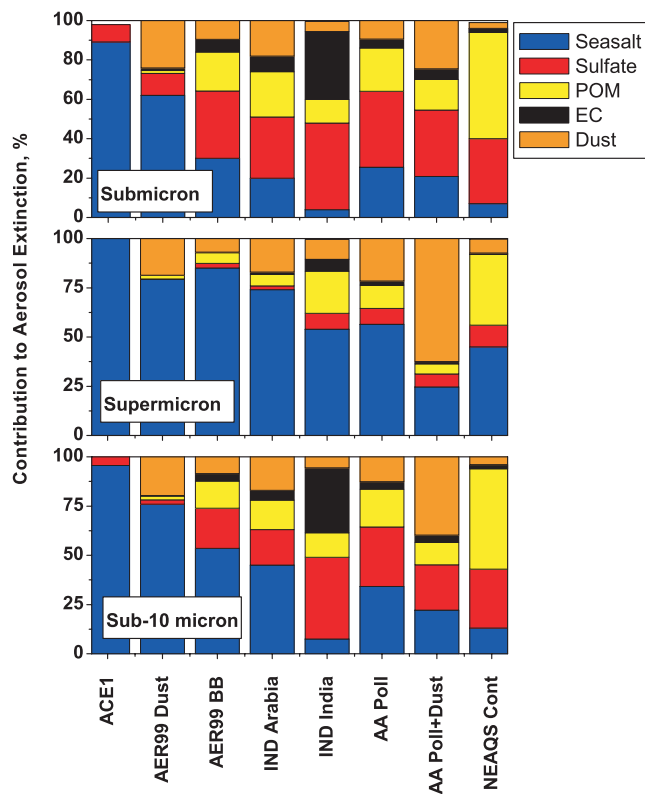


Figure 18. Mean regional extinction fractions of the dominant chemical components for the submicron, supermicron, and sub-10 μm size ranges. EC refers to elemental carbon, POM to particulate organic matter, and H_2O to the amount of water calculated to be associated with the inorganic ionic species at 55% RH.

by region. POM is a catchall for tens or hundreds of organic compounds within one region that have a range of hygroscopic properties. The definition of EC is based on the method used to quantify it. Here, we measured EC with a thermal optical technique, and hence it is the carbon that evolves above a certain temperature in a He/ O_2 mixture. The optical properties of EC depend on its mixing state with other chemical species, morphology, and chemical structure. The extinction fractions shown here are a first-order approximation, which can certainly be improved by a more thorough characterization of the properties of dust, POM, and EC including hygroscopicity, refractive index, and density.

4. Conclusions and Recommendations for the Future

4.1. Summary of Results

[89] The compilation of regional aerosol properties presented here provides a data set for the validation of chemical transport and radiative transfer models for specific times and locations. This series of aerosol experiments and the comparisons shown here have led to the following conclusions.

[90] 1. Sea salt dominates the sub- and supermicron aerosol mass and light extinction in remote marine atmospheres. In addition, in continental air masses that have

been transported into the marine atmosphere, the sea salt contribution to aerosol mass and light extinction is variable and almost always significant for all size ranges. This result indicates the necessity of including submicron sea salt in coupled chemical transport/radiative transfer models to provide accurate estimates of the radiative properties of the aerosol in marine environments.

[91] 2. A large fraction of the submicron aerosol mass in continental plumes is not sulfate. In these experiments, SO_4^{2-} made up, on average, 16 to 46% of the submicron aerosol mass at 55% RH. Hence the submicron mass is a complex mixture of sea salt, sulfate, POM, dust, and EC whose proportions depend on the sources impacting a particular region. As a consequence, light extinction by continental aerosol plumes is a result of a complex and highly variable mixture of chemical components for all size ranges.

[92] 3. POM is a ubiquitous and highly variable component in continental aerosol plumes. Mean submicron mass fractions over all regions ranged from 1 to 51% and supermicron mass fractions ranged from 1 to 21%. Highest mass fractions were found in the NE U.S. plume, perhaps due to the abundance of gas phase biogenic precursors such as isoprene and other reactive volatile organic compounds (VOCs).

[93] 4. Mean values of single-scattering albedo for sub-10 micron aerosol at ambient RH ranged from 0.89 to 0.99 for the continental plumes. Lowest values were found in biomass-burning plumes from Africa and plumes from the Indian subcontinent. The large reductions in solar radiation reaching the surface due to absorption by EC in the Indian haze may have significant impacts on the hydrological cycle [Ramanathan and Crutzen, 2003].

[94] 5. Relatively large single-scattering albedos were measured in the dust plumes emanating from the desert regions of Asia. The soot associated with the dust does not appear to have had a large effect on the single-scattering albedo of the dust-pollution mixture.

[95] 6. In marine environments, NO_3^- is almost entirely associated with coarse mode sea salt due to the reaction of HNO_3 and nonacidic gases such as NO_2 , ClONO_2 , and N_2O_5 with the sea salt. The transfer of NO_3^- from submicron to supermicron particles during transport over the oceans may also contribute to supermicron nitrate.

[96] 7. The range of regional mean values reported here for sub-10 μm single-scattering albedo (0.85 to 0.99) was estimated to result in a change of 8 W m^{-2} for TOA aerosol forcing efficiency.

[97] 8. The backscattered fraction of sub-10 micron aerosol is a complex function of particle size and shape. The range of mean values reported here (0.10 to 0.17) was estimated to result in a change of 9 W m^{-2} for TOA aerosol forcing efficiency.

[98] 9. Regional mean submicron mass scattering efficiencies for the total aerosol at 55% RH showed little variability ranging from 3.2 to $4.1 \text{ m}^2 \text{ g}^{-1}$. On the basis of these results, variability in the shape of the aerosol size distribution (modal diameter and width) is not large enough to lead to significant differences in submicron MSE. Similarly, mass extinction efficiencies for the dominant aerosol chemical components were consistent for all size ranges (with the exception of supermicron POM).

[99] 10. Regional mean sub-10 micron mass absorption efficiencies at 55% RH were highly variable, ranging from 5 to 30 m² g⁻¹. The observation of values above 10 m² g⁻¹, the theoretical Mie limit, suggests that either certain aerosol mixtures are not well described by Mie theory or there are instrumental issues with the thermo-optical analysis for EC and the filter-based absorption photometer that need to be better understood.

4.2. Identification of Measurement and Knowledge Gaps

[100] Not only have these experiments improved our knowledge about regional aerosol properties but they also have helped to point out current gaps in our knowledge. A partial list of areas for future research follows.

[101] 1. The significant contribution of sea salt to aerosol mass and extinction in almost all regions considered emphasizes the need for an accurate source function of sea salt aerosol for use in chemical transport models.

[102] 2. The discussion of a biomass/biofuel burning versus a fossil fuel combustion source of the IND India aerosol indicates the need for further measurements of EC and appropriate tracer species near sources and downwind of the continent. Ideally, these measurements should be systematic and routine and conducted from aircraft and at the surface.

[103] 3. Three of the major aerosol chemical components are not well characterized, which limits the accuracy of aerosol radiative forcing estimates. The shape and chemical composition of dust is highly variable. The scattering phase function of nonspherical particles is distinctly different than that of spheres [e.g., Kalashnikova and Sokolik, 2002]. Hence parameterizing the complex shape of dust in a meaningful way (i.e., on the basis of empirical data) is needed to quantify the optical properties of dust. Spectral light scattering and absorption by dust depends on its refractive index, density, and hygroscopicity. A thorough characterization of dust composition is required on a regional basis to determine the radiative forcing due to dust from different source regions. POM is composed of a multitude of organic species that vary in hygroscopicity. Functional group classification and speciation is required to understand and model the direct and indirect effects of POM. The light-absorbing properties of EC are variable owing to a range of morphologies, compositions, and mixing states with other chemical components. Characterization of the light-absorbing properties of EC based on source region and transformations during transport are required to better understand its impacts on climate.

4.3. Recommendations for Future Measurements

[104] Addressing these knowledge gaps and improving estimates of the impact of aerosols on climate and air quality requires a combination of laboratory work, intensive field campaigns, and long-term monitoring programs. Data presented in this paper are the result of a series of intensive field campaigns. We recommend that future intensives emphasize the following:

[105] 1. Measurements made on a time/space scale appropriate for understanding the effects of prevailing local, meso-, and synoptic scale meteorology. Instrument developments including particle-into-liquid-samplers [e.g., Sullivan

et al., 2004] and online aerosol mass spectrometers [e.g., Jayne *et al.*, 2000, Prather *et al.*, 1994] are making fast timescale measurements of aerosol chemical composition possible.

[106] 2. Measurements of gas and aerosol phase chemical species sufficient to determine aerosol sources (e.g., aerosol potassium and gas phase acetonitrile for the identification of a biomass-burning source of EC).

[107] 3. Measurements of particulate organic matter to characterize its source, formation processes, composition, and cloud nucleating abilities.

[108] 4. In situ measurements of aerosol absorption and extinction using emerging technologies such as photoacoustic and cavity ring down methods.

[109] 5. Statistical modeling of dust morphology based on empirical measurements [e.g., Kalashnikova and Sokolik, 2002].

[110] 6. Collection of overdetermined data sets so that a measured parameter (such as aerosol mass or light extinction) can be compared to the same parameter calculated from an independent set of measurements.

[111] 7. Identification and quantification of measurement uncertainties so that they can be included in comparisons with modeled parameters.

[112] 8. Coupling of high-resolution models with measurements (e.g., through validation and assimilation).

[113] In addition to intensive field experiments, long-term measurements at fixed surface sites and from aircraft in strategic locations over and downwind of aerosol source regions are needed to provide a broader context for “snapshot” intensives and for ground truthing satellites that are coming online. We recommend that the longer-term measurements emphasize standardized measurement protocols to remove sampling biases and make the data from around the world directly comparable.

[114] Laboratory work is required to accomplish the following:

[115] 1. Develop sizing instruments capable of characterizing the size and shape of large particles.

[116] 2. Systematically measure optical properties of aerosol mixtures (e.g., absorption, scattering, and refractive index) and properties that affect cloud-nucleation (e.g., surface tension, water activity, uptake of soluble gases).

[117] 3. Characterize in situ instruments prior to going into the field so that their response to the measured aerosol (e.g., composition and morphology) is understood.

[118] 4. Perform preintensive comparisons and calibrations of similar instruments that will be deployed on multiple platforms during intensives so that data are directly comparable.

[119] Although the impact of aerosols on climate and air quality is largely a regional scale problem, it can be expanded to a global scale through intercontinental long-range transport. A global aerosol observing system comprised of regional measurements (both intensive and long term) is required to understand the impact of the long-range transport of aerosols. Development of a global data base of measured regional aerosol properties would aid in this goal.

[120] Our understanding of regional aerosols, ranging from remote marine to complex pollution-dust mixtures, has improved tremendously over the past decade. In addition, in situ measurements techniques have advanced significantly

in their time and size resolution and ability to characterize the chemical and physical properties of the aerosol. These new techniques combined with the approach of collecting overdetermined data sets and emphasizing instrument and model comparisons in the laboratory and in the field, will lead to significant advances in our understanding of the climate and health impacts of aerosol in the next decade.

[121] **Acknowledgments.** We thank D. Coffman, D. Covert, D. Hamilton, J. Johnson, and T. Miller for logistical and technical assistance and the officers and crew of the NOAA research vessels involved in these projects. This research was funded by NOAA OGP's Aerosol Program. This is NOAA PMEL contribution number 2684 and JISAO contribution number 1053.

References

- Ackerman, A. S., O. B. Toon, D. E. Stevens, A. J. Heymsfield, V. Ramanathan, and E. J. Welton (2000), Reduction of tropical cloudiness by soot, *Science*, *288*, 1042–1047.
- Alfaro, S. C., et al. (2003), Chemical and optical characteristics of aerosols measured in spring 2002 at the ACE-Asia supersite, Zhenbeitai, China, *J. Geophys. Res.*, *108*(D23), 8641, doi:10.1029/2002JD003214.
- Anderson, T. L., and J. A. Ogren (1998), Determining aerosol radiative properties using the TSI 3563 integrating nephelometer, *Aeron. Sci. Technol.*, *29*, 57–69.
- Anderson, T. L., et al. (2003), Variability of aerosol optical properties derived from in situ aircraft measurements during ACE Asia, *J. Geophys. Res.*, *108*(D23), 8647, doi:10.1029/2002JD003247.
- Andreae, M. O. (1983), Soot carbon and excess fine potassium: Long-range transport of combustion-derived aerosols, *Science*, *220*, 1148–1151.
- Andreae, M. O., and P. Merlet (2001), Emission of trace gases and aerosols from biomass burning, *Global Biogeochem. Cycles*, *15*, 955–966.
- Andreae, M. O., et al. (1998), Airborne studies of aerosol emissions from savanna fires in southern Africa: 2. Aerosol chemical composition, *J. Geophys. Res.*, *103*, 32,119–32,128.
- Bates, T. S., B. J. Huebert, J. L. Gras, F. B. Griffiths, and P. A. Durkee (1998a), International Global Atmospheric Chemistry (IGAC) project's first Aerosol Characterization Experiment (ACE 1): Overview, *J. Geophys. Res.*, *103*, 16,297–16,318.
- Bates, T. S., V. N. Kapustin, P. K. Quinn, D. S. Covert, D. J. Coffman, C. Mari, P. A. Durkee, W. DeBruyn, and E. Saltzman (1998b), Processes controlling the distribution of aerosol particles in the marine boundary layer during ACE-1, *J. Geophys. Res.*, *103*, 16,369–16,383.
- Bates, T. S., P. K. Quinn, D. S. Covert, D. J. Coffman, J. E. Johnson, and A. Wiedensohler (2000), Aerosol physical properties and controlling processes in the lower marine boundary layer: A comparison of submicron data from ACE-1 and ACE-2, *Tellus*, *52B*, 258–272.
- Bates, T. S., P. K. Quinn, D. J. Coffman, J. E. Johnson, T. L. Miller, D. S. Covert, A. Wiedensohler, S. Leinert, A. Nowak, and C. Neususs (2001), Regional physical and chemical properties of the marine boundary layer aerosol across the Atlantic during Aerosols99: An overview, *J. Geophys. Res.*, *106*, 20,767.
- Bates, T. S., D. J. Coffman, D. S. Covert, and P. K. Quinn (2001), Regional marine boundary layer aerosol size distributions in the Indian, Atlantic, and Pacific Oceans: A comparison of INDOEX measurements with ACE-1, ACE-2, and Aerosols99, *J. Geophys. Res.*, *107*(D18), 8026, doi:10.1029/2001JD001174.
- Bates, T. S., et al. (2004), Marine boundary layer dust and pollution transport associated with the passage of a frontal system over eastern Asian, *J. Geophys. Res.*, *109*, D19S19, doi:10.1029/2003JD004094.
- Bergametti, G., L. Gomes, G. Coude-Gaussen, P. Rognon, and M.-N. Le Coustumer (1989), African Dust observed over Canary Islands: Source-regions identification and transport pattern for some summer situations, *J. Geophys. Res.*, *94*, 14,855–14,864.
- Berner, A., C. Lurzer, F. Pohl, O. Preining, and P. Wagner (1979), The size distribution of the urban aerosol in Vienna, *Sci. Total Environ.*, *13*, 245–261.
- Birch, M. E., and R. A. Cary (1996), Elemental carbon-based method for monitoring occupational exposures to particulate diesel exhaust, *Aerosol Sci. Technol.*, *25*, 221–241.
- Bond, T. C., T. L. Anderson, and D. Campbell (1999), Calibration and intercomparison of filter-based measurements of visible light absorption by aerosols, *Aerosol Sci. Technol.*, *30*, 582–600.
- Bond, T. C., D. G. Streets, K. F. Yarber, S. M. Nelson, J.-H. Woo, and Z. Klimont (2004), A technology-based global inventory of black and organic carbon emissions from combustion, *J. Geophys. Res.*, *109*, D14203, doi:10.1029/2003JD003697.
- Cahill, T. A., R. A. Eldred, and P. J. Feeney (1986), Particulate monitoring and data analysis for the National Park Service, 1982–1985, Univ. of Calif., Davis, Calif.
- Carrico, C., M. Rood, and J. Ogren (1998), Aerosol light scattering properties at Cape Grim, Tasmania, during the First Aerosol Characterization Experiment (ACE 1), *J. Geophys. Res.*, *103*, 16,565–16,574.
- Carrico, C. M., M. J. Rood, J. A. Ogren, C. Neusses, A. Wiedensohler, and J. Heintzenberg (2000), Aerosol optical properties at Sagre, Portugal during ACE-2, *Tellus*, *52B*, 694–715.
- Carrico, C., P. Kus, M. Rood, P. Quinn, and T. Bates (2003), Mixtures of pollution, dust, seasalt, and volcanic aerosol during ACE-Asia: Aerosol radiative properties as a function of relative humidity, *J. Geophys. Res.*, *108*(D23), 8650, doi:10.1029/2003JD003405.
- Chuang, P. Y., R. M. Duvall, M. S. Bae, A. Jefferson, J. J. Schauer, H. Yang, J. Z. Yu, and J. Kim (2003), Observations of elemental carbon and absorption during ACE-Asia and implications for aerosol radiative properties and climate forcing, *J. Geophys. Res.*, *108*(D23), 8634, doi:10.1029/2002JD003254.
- Clegg, S. L., and P. Brimblecombe (1985), Potential degassing of hydrogen chloride from acidified sodium chloride droplets, *Atmos. Environ.*, *19*, 465–470.
- Collins, W. D., et al. (2001), Simulating aerosols using a chemical transport model with assimilation of satellite aerosol retrievals: Methodology for INDOEX, *J. Geophys. Res.*, *106*, 7313–7336.
- Cooke, W. F., C. Liousse, and H. Cachier (1999), Construction of a $1^\circ \times 1^\circ$ fossil fuel emission data set for carbonaceous aerosol and implementation and radiative impact in the ECHAM4 model, *J. Geophys. Res.*, *104*, 22,137–22,162.
- Dickerson, R. R., M. O. Andreae, T. Campos, O. L. Mayol-Bracero, C. Neusuess, and D. G. Streets (2002), Analysis of black carbon and carbon monoxide observed over the Indian Ocean: Implications for emissions and photochemistry, *J. Geophys. Res.*, *107*(D19), 8017, doi:10.1029/2001JD000501.
- Draxler, R. R. (1992), Hybrid Single-Particle Lagrangian Integrated Trajectories (HY-SPLIT): version 3.0. user's guide and model description, *Tech. Rep. ERL ARL-195*, NOAA, Silver Spring, Md.
- Feely, R. A., G. J. Massoth, and G. T. Lebon (1991), Sampling of marine particulate matter and analysis by X-ray fluorescence spectrometry, in *Marine Particles: Analysis and Characterization*, *Geophys. Monogr. Ser.*, vol. 63, edited by D. C. Hurd and D. W. Spencer, pp. 251–257, AGU, Washington, DC.
- Feely, R. A., E. T. Baker, G. T. Lebon, J. F. Gendron, G. J. Massoth, and C. W. Mordy (1998), Chemical variations of hydrothermal particles in the 1996 Gorda Ridge Event and chronic plumes, *Deep Sea Res.*, *45*, 2637–2664.
- Ferek, R. J., J. S. Reid, P. V. Hobbs, D. R. Blake, and C. Liousse (1998), Emission factors of hydrocarbons, trace gases and particles from biomass burning in Brazil, *J. Geophys. Res.*, *103*, 32,107–32,118.
- Finlayson-Pitts, B. J. (1983), Reaction of NO₂ with NaCl and atmospheric implications of NOCl formation, *Nature*, *306*, 676–677.
- Finlayson-Pitts, B. J., M. J. Ezell, and J. N. Pitts Jr. (1989), Formation of chemically active chlorine compounds by reactions of atmospheric NaCl particles with gaseous N₂O₅ and ClONO₂, *Nature*, *337*, 241–244.
- Fuller, K. A., W. C. Malm, and S. M. Kreidenweis (1999), Effects of mixing on extinction by carbonaceous particles, *J. Geophys. Res.*, *104*, 15,941–15,954.
- Gaudichet, A., F. Echalar, B. Chatenet, J. P. Quisefit, G. Malingre, H. Cachier, P. Buat-Menard, P. Artaxo, and W. Maenhaut (1995), Trace elements in tropical African Savanna biomass-burning aerosols, *J. Atmos. Chem.*, *22*(1–2), 19–39.
- Gomes, L., and D. A. Gillette (1993), A comparison of characteristics of aerosol from dust storms in Central Asia with soil-derived dust from other regions, *Atmos. Environ., Part A*, *27*, 2539–2544.
- Gong, S. L., L. A. Barrie, and J.-P. Blanchet (1997), Modeling sea-salt aerosols in the atmosphere: 1. Model development, *J. Geophys. Res.*, *102*, 3805–3818.
- Guazzotti, S. A., D. T. Suess, K. R. Coffee, K. A. Prather, P. K. Quinn, T. S. Bates, W. P. Ball, R. R. Dickerson, C. Neususs, and P. Crutzen (2003), Characterization of carbonaceous aerosols outflow from India and Arabia: Biomass/biofuel burning and fossil fuel combustion, *J. Geophys. Res.*, *108*(D15), 4485, doi:10.1029/2002JD003277.
- Guenther, A., et al. (1995), A global model of natural volatile organic compound emissions, *J. Geophys. Res.*, *100*, 8873–8892.
- Haywood, J. M., and K. P. Shine (1995), The effect of anthropogenic sulfate and soot aerosol on the clear sky planetary radiation budget, *Geophys. Res. Lett.*, *22*, 603–606.
- Hegg, D. A., et al. (1997), Chemical apportionment of aerosol column optical depth off the mid-Atlantic coast of the United States, *J. Geophys. Res.*, *102*, 25,293–25,303.

- Holland, H. D. (1978), *The Chemistry of the Atmosphere and Oceans*, p. 154, John Wiley, Hoboken, N. J.
- Huebert, B. J., T. Bates, P. Russell, G. Shi, Y. J. Kim, and K. Kawamura (2003), An overview of ACE Asia: Strategies for quantifying the relationships between Asian aerosols and their climatic impacts, *J. Geophys. Res.*, *108*(D23), 8633, doi:10.1029/2003JD003550.
- Intergovernmental Panel on Climate Change (IPCC) (1996), *Climate Change 1995*, edited by J. T. Houghton et al., Cambridge Univ. Press, New York.
- Intergovernmental Panel on Climate Change (IPCC) (2001), *Climate Change 2001*, edited by J. T. Houghton et al., Cambridge Univ. Press, New York.
- Jayne, J. T., D. C. Leard, X. Zhang, P. Davidovits, K. A. Smith, C. E. Kolb, and D. R. Worsnop (2000), Development of an aerosol mass spectrometer for size and composition: Analysis of submicron particles, *Aerosol Sci. Technol.*, *33*, 49–70.
- Kalashnikova, O. V., and I. N. Sokolik (2002), Importance of shapes and compositions of wind-blown dust particles for remote sensing at solar wavelengths, *Geophys. Res. Lett.*, *29*(10), 1398, doi:10.1029/2002GL014947.
- Kaneyasu, N., S. Ohta, and N. Muraio (1995), Seasonal variation in the chemical composition of atmospheric aerosols and gaseous species in Sapporo, Japan, *Atmos. Environ.*, *29*(13), 1559–1568.
- Keene, W. C., A. A. P. Pszenny, D. J. Jacob, R. A. Duce, J. N. Galloway, J. J. Schultz-Tokos, H. Sievering, and J. F. Boatman (1990), The geochemical cycling of reactive chlorine through the marine troposphere, *Global Biogeochem. Cycles*, *4*, 407–430.
- Kim, U. P., K. C. Moon, J. H. Lee, and N. J. Baik (1999), Concentrations of carbonaceous species in particles at Seoul and Cheju in Korea, *Atmos. Environ.*, *33*, 2751–2758.
- Kleeman, M. J., J. J. Schauer, and G. R. Cass (2000), Size and composition of fine particulate matter emitted from motor vehicles, *Environ. Sci. Technol.*, *34*, 1132–1142.
- Kotchenruther, R. A., P. V. Hobbs, and D. A. Hegg (1999), Humidification factors for atmospheric aerosols off the mid-Atlantic coast of the United States, *J. Geophys. Res.*, *104*, 2239–2251.
- Langner, J., and H. Rodhe (1991), A global three-dimensional model of the tropospheric sulphur cycle, *J. Atmos. Chem.*, *13*, 255–263.
- Li-Jones, X., H. B. Maring, and J. M. Prospero (1998), Effect of relative humidity on light scattering by mineral dust aerosol as measured in the marine boundary layer over the tropical Atlantic Ocean, *J. Geophys. Res.*, *103*, 31,113–31,121.
- Liousse, C., J. E. Penner, C. Chuang, J. J. Walton, and H. Eddleman (1996), A global three-dimensional study of carbonaceous aerosol, *J. Geophys. Res.*, *101*, 19,411–19,432.
- Livingston, J. M., et al. (2000), Shipboard sunphotometer measurements of aerosol optical depth spectra and columnar water vapor during ACE 2 and comparison with selected land, ship, aircraft, and satellite measurements, *Tellus*, *52B*, 594–619.
- Lobert, J., M. D. H. Scharffe, W. M. Hao, and P. J. Crutzen (1990), Importance of biomass burning in the atmospheric budgets of nitrogen-containing gases, *Nature*, *347*, 552–554.
- Maenhaut, W., I. Salma, J. Cafmeyer, H. J. Annegarn, and M. O. Andreae (1996), Regional atmospheric aerosol composition and sources in the eastern Transvaal, South Africa, and impact of biomass burning, *J. Geophys. Res.*, *101*, 23,631–23,650.
- Magi, B. I., and P. V. Hobbs (2003), Effects of humidity on aerosols in southern Africa during the biomass burning season, *J. Geophys. Res.*, *108*(D13), 8495, doi:10.1029/2002JD002144.
- Malm, W. C., J. F. Sisler, D. Huffman, R. A. Eldred, and T. A. Cahill (1994), Spatial and seasonal trends in particle concentration and optical extinction in the United States, *J. Geophys. Res.*, *99*, 1347–1370.
- Martins, J. V., P. Artaxo, C. Liousse, J. S. Reid, P. V. Hobbs, and Y. J. Kaufman (1998), Effects of black carbon content, particle size, and mixing on light absorption by aerosols from biomass burning in Brazil, *J. Geophys. Res.*, *103*, 32,041–32,050.
- McGovern, F. M., M. J. Nunes, F. Raes, and H. Gonzales-Jorge (2002), Marine and anthropogenic aerosols at Punta Del Hildalgo, Tenerife, and the aerosol nitrate number paradox, *J. Geophys. Res.*, *107*(D24), 4766, doi:10.1029/2001JD000827.
- McInnes, L., M. Bergin, J. Ogren, and S. Schwartz (1998), Apportionment of light scattering and hygroscopic growth to aerosol composition, *Geophys. Res. Lett.*, *25*, 513–516.
- Neusüß, C., T. Gnauk, A. Plewka, H. Herrmann, and P. K. Quinn (2002), Carbonaceous aerosol over the Indian Ocean: OC/EC fractions and selected specifications from size-segregated samples taken onboard the R/V Ron Brown, *J. Geophys. Res.*, *107*(D19), 8031, doi:10.1029/2001JD000327.
- Novakov, T., D. A. Hegg, and P. V. Hobbs (1997), Airborne measurements of carbonaceous aerosols on the east coast of the United States, *J. Geophys. Res.*, *102*, 30,023–30,030.
- Novakov, T., T. S. Bates, and P. K. Quinn (2000), Shipboard measurements of concentrations and properties of carbonaceous aerosols during ACE-2, *Tellus*, *52B*, 228–238.
- Perry, K. D., T. A. Cahill, R. A. Eldred, D. D. Dutcher, and T. E. Gill (1997), Long-range transport of North African dust to the eastern United States, *J. Geophys. Res.*, *102*, 11,225–11,238.
- Prather, K. A., T. Nordmeyer, and K. Salt (1994), Real-time characterization of individual aerosol particles using time-of-flight mass spectrometry, *Anal. Chem.*, *66*, 1403–1407.
- Putaud, J. P., et al. (2000), Chemical mass closure and assessment of the origin of the submicron aerosol in the marine boundary layer and the free troposphere at Tenerife during ACE-2, *Tellus*, *52B*, 141–168.
- Quinn, P. K., and T. S. Bates (2003), North American, Asian, and Indian haze: Similar regional impacts on climate?, *Geophys. Res. Lett.*, *30*(11), 1555, doi:10.1029/2003GL016934.
- Quinn, P. K., and D. J. Coffman (1998), Local closure during ACE 1: Aerosol mass concentration and scattering and backscattering coefficients, *J. Geophys. Res.*, *103*, 16,575–16,596.
- Quinn, P. K., and D. J. Coffman (1999), Comment on “Contribution of different aerosol species to the global aerosol extinction optical thickness: Estimates from model results” by Tegen et al., *J. Geophys. Res.*, *104*, 4241–4248.
- Quinn, P. K., D. J. Coffman, V. N. Kapustin, T. S. Bates, and D. S. Covert (1998), Aerosol optical properties in the marine boundary layer during ACE 1 and the underlying chemical and physical aerosol properties, *J. Geophys. Res.*, *103*, 16,547–16,563.
- Quinn, P. K., et al. (2000a), Surface submicron aerosol chemical composition: What fraction is not sulfate?, *J. Geophys. Res.*, *105*, 6785–6806.
- Quinn, P. K., T. S. Bates, D. J. Coffman, T. L. Miller, J. E. Johnson, D. S. Covert, J. P. Putaud, C. Nesusseus, and T. Novakov (2000b), A comparison of aerosol chemical and optical properties from the first and second aerosol characterization experiments, *Tellus*, *52B*, 239–257.
- Quinn, P. K., D. J. Coffman, T. S. Bates, T. L. Miller, J. E. Johnson, K. Voss, E. J. Welton, and C. Neusüss (2001), Dominant aerosol chemical components and their contribution to extinction during Aerosols99 cruise across the Atlantic, *J. Geophys. Res.*, *106*, 20,783.
- Quinn, P. K., D. J. Coffman, T. S. Bates, T. L. Miller, J. E. Johnson, E. J. Welton, C. Neusüss, M. Miller, and P. Sheridan (2002), Aerosol optical properties during INDOEX 1999: Means, variabilities, and controlling factors, *J. Geophys. Res.*, *107*(D19), 8020, doi:10.1029/2000JD000037.
- Quinn, P. K., et al. (2004), Aerosol optical properties measured onboard the *Ronald H. Brown* during ACE Asia as a function of aerosol chemical composition and source region, *J. Geophys. Res.*, *109*, D19S01, doi:10.1029/2003JD004010.
- Raes, F., T. S. Bates, F. McGovern, and M. Vanliedekerke (2000), The second Aerosol Characterization Experiment (ACE-2): General overview and main results, *Tellus*, *52*, 111–125.
- Ramanathan, V., and P. J. Crutzen (2003), New directions: Atmospheric brown clouds, *Atmos. Environ.*, *37*, 4033–4035.
- Ramanathan, V., et al. (2001), Indian Ocean Experiment: An integrated analysis of the climate forcing and effects of the great Indo-Asian haze, *J. Geophys. Res.*, *106*, 28,371–28,398.
- Rasch, P. J., W. D. Collins, and B. E. Eaton (2001), Understanding the Indian Ocean Experiment (INDOEX) aerosol distributions with an aerosol assimilation, *J. Geophys. Res.*, *106*, 7337–7355.
- Remer, L. A., Y. J. Kaufman, and B. N. Holben (1999), Interannual variation of ambient aerosol characteristics on the east coast of the United States, *J. Geophys. Res.*, *104*, 2223–2231.
- Reddy, M. S., and Venkataraman (2002), Inventory of aerosol and sulphur dioxide emissions from India, I, Fossil fuel combustion, *Atmos. Environ.*, *36*, 677–697.
- Ruellan, S., H. Cachier, A. Gaudichet, P. Masselet, and J. P. Lacaux (1999), Airborne aerosols over central Africa during Experiment for Regional Sources and Sinks of Oxidants (EXPRESSO), *J. Geophys. Res.*, *104*, 30,673–30,690.
- Russell, P. B., P. V. Hobbs, and L. L. Stowe (1999), Aerosol properties and radiative effects in the United States East Coast haze plume: An overview of the Tropospheric Aerosol Radiative Forcing Observational Experiment {TARFOX}, *J. Geophys. Res.*, *104*, 2213–2222.
- Satheesh, S. K., and V. Ramanathan (2000), Large differences in the tropical aerosol forcing at the top of the atmosphere and Earth’s surface, *Nature*, *405*, 60–63.
- Seinfeld, J. H. (1986), *Atmospheric Chemistry and Physics of Air Pollution*, p. 296, John Wiley, Hoboken, N. J.
- Shaw, M. A., and M. J. Rood (1990), Measurement of the crystallization humidities of ambient aerosol particles, *Atmos. Environ.*, *24A*, 1837–1841.
- Sheridan, P. J., and J. A. Ogren (1999), Observations of the vertical and regional variability of aerosol optical properties over central and eastern North America, *J. Geophys. Res.*, *104*, 16,793–16,805.

- Smirnov, A., et al. (2002), Optical properties of atmospheric aerosol in maritime environments, *J. Atmos. Sci.*, *59*, 501–523.
- Sullivan, A. P., R. J. Weber, A. L. Clements, J. R. Turner, M. S. Bae, and J. J. Schauer (2004), A method for on-line measurement of water-soluble organic carbon in ambient aerosol particles: Results from an urban site, *Geophys. Res. Lett.*, *31*, L13105, doi:10.1029/2004GL019681.
- Tang, I. N., A. C. Tridico, and K. H. Fung (1997), Thermodynamic and optical properties of sea-salt aerosol, *J. Geophys. Res.*, *102*, 23,269–23,275.
- Turpin, B. J., and H. Lim (2001), Species contribution to PM_{2.5} concentrations: Revisiting common assumptions for estimating organic mass, *Aeron. Sci. Technol.*, *35*, 602–610.
- Turpin, B. J., J. J. Huntzicker, and S. V. Hering (1994), Investigation of organic aerosol sampling artifacts in the Los Angeles Base, *Atmos. Environ.*, *28*, 23,061–23,071.
- Turpin, B. J., P. Saxena, and E. Andrews (2000), Measuring and simulating particulate organics in the atmosphere: Problems and prospects, *Atmos. Environ.*, *34*, 2983–3013.
- Voss, K. J., E. J. Welton, P. K. Quinn, R. Frouin, M. Miller, and R. M. Reynolds (2001), Aerosol Optical Depth measurements during the Aerosols99 experiment, *J. Geophys. Res.*, *106*, 20,811.
- Welton, E. J., K. J. Voss, P. K. Quinn, J. R. Campbell, P. J. Flatau, J. D. Spinhirne, K. Markowicz, H. R. Gordon, and J. Johnson (2002), Measurements of aerosol vertical profiles and optical properties during INDOEX 1999 using micro-pulse lidars, *J. Geophys. Res.*, *107*(D19), 8019, doi:10.1029/2000JD000038.
- Wiscombe, W. J., and G. W. Grams (1976), The backscattered fraction in two-stream approximations, *J. Atmos. Sci.*, *33*, 2440–2451.

T. S. Bates and P. K. Quinn, Pacific Marine Environment Laboratory, NOAA, 7600 Sand Point Way NE, Seattle, WA 98115, USA. (patricia.k.quinn@noaa.gov)